Mantle heterogeneity generated by melt depletion and melt-rock interaction: the West Iberian margin peridotites (ODP Leg 149 and 173).

Arianna Secchiari[1*], Marguerite Godard[2], Alessandra Montanini[3]

[1] Earth Sciences Dept. "A. Desio", University of Milan, Italy

[2] Géosciences Montpellier, CNRS, University of Montpellier, France

[3] Department of Chemistry, Life Sciences and Environmental Sustainability, University of Parma, Italy

*Corresponding author: Arianna Secchiari, arianna.secchiari@unimi.it

ABSTRACT

Understanding the nature and evolution of mantle sequences exhumed along modern magma-poor ocean-continent transition zones (OCTs) is essential for deciphering the complex interplay of tectonic and magmatic processes from rifting to oceanization. However, the data on these specific tectonic settings remain limited. In this study, we revisit peridotites from the West Iberian margin (WIM) through a petrological and geochemical investigation of mantle exposures sampled in the Iberia Abyssal Plain (IAP). We focus on three ODP sites constituting an east-to-west transect, from Hole 1068A to Holes 899B and the westernmost Hole 1070A, to capture the full spectrum of mantle variability from the continental to the most oceanward domains. The analysed samples consist of variably serpentinized, coarse-grained peridotites preserving evidence of melt-rock interactions.

In Hole 1068A, strongly serpentinized plagioclase lherzolites are found. Mineral chemistry, i.e., high Cr# and TiO_2 in spinel, along with Na_2O- and Al_2O_3-enriched clinopyroxene, indicate that these samples are akin to impregnated peridotites from the sub-continental lithospheric mantle (SCLM). Geochemical modelling based on clinopyroxene REE compositions points to refertilization processes driven by MORB-type melts.

In contrast, Hole 899B displays more pronounced variability and apparently contrasting geochemical features. Spinel harzburgites (cpx ~ 2-3 vol.%) exhibit evidence of olivine-forming, pyroxene-dissolving microstructures. Their slightly depleted clinopyroxene compositions (Na_2O= 0.23-0.60 wt. %), combined with atypical chondrite-normalized V-shaped REE patterns, suggest that these rocks experienced partial melting followed by interaction with LREE-enriched melts. These peridotites may represent inherited SCLM, or a refractory peridotite modified by rifting-related melts. One sample however, plagioclase harzburgite 899-1 (cpx ~ 8 vol.%), is distinguished by peculiar microtextures—such as opx2±pl aggregates replacing olivine porphyroclasts— and spinel compositions (TiO_2 up to 0.6 wt. %), that indicate late melt/rock impregnation. The concave-downward clinopyroxene REE patterns point to interaction with a depleted melt.

Hole 1070A spinel harzburgites (cpx ~ 2-5 vol.%) exhibit the most distinctive features. Their low clinopyroxene content, with a positive correlation between Cr#, Al_2O_3 and Yb, suggests that these peridotites represent a suite of partial melting residues. However, the unusual Cr-Na enrichments and the rare hump-shaped clinopyroxene REE patterns cannot be solely ascribed to melt depletion. These characteristics reflect open-system melting within the spinel stability field, accompanied by the influx of an enriched melt generated in the garnet stability field. This process likely occurred during the deep lithospheric mantle's transition from rifting to oceanization.

Calculated equilibrium temperatures for the WIM peridotites fall within the range of fossil OCTs ($T_{Ca\text{-}in\text{-}Opx}$= 921-1029 °C). As a whole, they indicate a high-temperature history ($T_{REE\text{-}Y}$= 1098-1244 °C) related to melt-rock interaction, followed by slow thermal re-equilibration ($T_{Ol\text{-}Sp}$= 770-813 °C).

Our new data provide compelling evidence for mantle heterogeneity in the WIM, observed both among different drill sites and within the same borehole. Our study challenges the classical and simplified perspective of OCTs as regions characterized by a fixed distribution of mantle domains with clearly defined chemical compositions. Instead, we propose that OCTs are composed of a complex mosaic of mantle signatures, reflecting superimposition of recent processes related to rifting and oceanization over an earlier, and possibly ancient, evolutionary history.

INTRODUCTION

Magma-poor ocean-continent transitions (OCTs) encompass wide areas of tectonically exhumed mantle emplaced during the late-stage rifting evolution. While a substantial body of literature have dealt with the investigation of fossil analogues (e.g. Manatschal & Müntener, 2009; Muntener *et al.*, 2004, 2010; Montanini *et al.*, 2006 ; Ferrari *et al.*, 2022; see also Picazo et *al.*, 2016 and references therein), studies on mantle sequences exhumed in modern OCTs remain limited (e.g. Abe, 2001; Hébert *et al.*, 2001; Chazot *et al.*, 2005; McCarthy *et al.*, 2020). This can be attributed to the difficulties associated with accessing and sampling the peridotite basement in these specific settings, primarily due to the challenges posed by ultra-deep-water drilling. The scarcity of available data and information on these systems contributes to our fragmented understanding on their tectono-magmatic evolution. Key questions that remain hotly debated include the mechanisms, location, and timing of lithospheric breakup and melt production, as well as the nature of the mantle sources involved.

Among continental margins worldwide, the West Iberian margin (WIM) stands out as one of the best-documented sites where mantle has been first accessed through scientific drilling more than three decades ago (Boillot *et al.*, 1989). However, the study of mantle rocks in this region has received limited attention, primarily due to their extensive serpentinization, which has hindered a comprehensive geochemical characterization. As a result, the existing studies on peridotites from the WIM remain relatively scarce and, with only a few exceptions (Abe, 2001; Chazot *et al.*, 2005; Hebert *et al.*, 2001), mostly based on mineral major element analysis (Whitmarsh & Sawyer, 1996; Cornen *et al.*, 1996). Previous petrological investigations have interpreted the mantle rocks in this area either as remnants of SCLM (Hébert *et al.*, 2001; Chazot *et al.*, 2005) or asthenospheric mantle accreted to the lithosphere and emplaced at shallow depths in a relatively cool regime during the continental lithosphere thinning (Cornen *et al.*, 1996a). Intriguingly, these studies have revealed the coexistence of refractory harzburgites, and fertile plagioclase-bearing peridotites exposed along the OCT of the WIM. Various hypotheses have been proposed to explain the origin and evolution of these mantle rocks. Abe (2001) suggested that the refractory harzburgites might have resulted from open-system melting during plume-assisted rifting of the continental margin. On the other hand, in the same study Abe (2001) noted similarities between the WIM peridotites and arc xenoliths from Japan, raising the hypothesis that the WIM harzburgites could have undergone supra-subduction zone processes as part of the former Ibero-Armorican Arc. Chazot and coauthors (2005) also proposed that the refractory compositions of these harzburgites might not be linked to the recent rifting evolution. They interpreted the residual nature of these mantle rocks as inherited from a previous melting evolution, potentially associated with or predating the

Variscan orogeny.

Similarly, the plagioclase-bearing peridotites have been subject to contrasting interpretations, with some authors suggesting a sub-solidus re-equilibration origin for plagioclase (Abe, 2001; Chazot *et al.*, 2005), while others arguing for its formation through melt impregnation (Cornen *et al.*, 1996a; Hébert *et al.*, 2001).

The nature and evolution of the WIM peridotites have thus remained puzzling, presenting an enduring enigma that demands further investigation. To address this knowledge gap, we carried out a combined petrological and geochemical study on a new set of mantle rocks from ODP Leg 149 and 173, located in the Iberia Abyssal Plain (IAP). To provide a comprehensive overview of mantle heterogeneity in the WIM, we have revisited these drill sites in light of recent models proposed for these mantle sequences (Péron-Pinvidic *et al.*, 2007; Tucholke *et al.*, 2007; Péron-Pinvidic & Manatschal, 2009). We focused on peridotite drill sites, ranging from the most continental to the most oceanward mantle domains. Three different boreholes were targeted along an east-to-west transect: (1) ODP Hole 1068A, (2) Hole 899B, and (3) Hole 1070A.

To minimize the effects of serpentinization, our investigation has been based exclusively on an in-situ characterization. Through this work we aim to: (i) decipher the nature of the peridotite basement exposed in the WIM; (ii) trace the evolution and processes undergone by these mantle rocks; (iii) compare our new findings with previously proposed models for OCTs; (iv) advance the current understanding of magma-poor ocean-continent transitions.

GEOLOGY

The South Iberia Abyssal Plain (IAP): geological setting and site characteristics

The WIM is the continental rifted margin marking the western edge of the Iberian Peninsula. From north to south, the margin can be divided into three main segments (Fig. 1): (i) the Galicia margin; (ii) the Iberia Abyssal Plain and (iii) the Tago Abyssal Plain. This segmentation resulted from the Early Cretaceous rifting and continental breakup between the North American and European/Iberian plates (see Whitmarsh & Wallace, 2001 and references therein). As a sediment-starved margin, the WIM has been the object of several investigations, and it is presently regarded as the most iconic example of a magma-poor (non-volcanic) passive margin. Combined geophysical surveys, submersible diving and drilling have revealed that much of the IAP basement consists of serpentinized peridotites and of tilted fault blocks of continental crust (Boillot *et al.*, 1987; Whitmarsh & Sawyer, 1996; Whitmarsh *et al.*, 1998). Mantle uplift and exhumation to the seafloor has been attributed to amagmatic continental rifting (Whitmarsh *et al.*, 2001) and to late hyper-extensive tectono-magmatic mechanisms marking the limit of the oceanic to continental domains (Péron-Pinvidic & Manatschal, 2009). The WIM peridotite basement crops out in the OCT and extends across a ~ 100-km-wide area (Minshull *et al.*, 2014). During ODP Leg 149 and 173, peridotites were recovered at different sites. We selected ten peridotite samples recovered from ODP Holes 1068A, 899B and 1070A (Table 1). Sampled intervals were selected based on previous literature and/or shipboard reports indicating the occurrence of preserved lithologies and/or mineral relics. Thereafter, we briefly report the main characteristics of the investigated boreholes, primarily based on Whitmarsh *et al.* (1996, 1998) and Whitmarsh & Wallace (2001). For each borehole, the lithostratigraphy and sample location is illustrated in Supplementary Fig. S1.

Hole 1068A

Hole 1068A lies near the southern edge of the Iberia Abyssal Plain (Supplementary Fig. S1a): it is the closest sampling site to the Iberia peninsula where mantle has been accessed. The borehole penetrated to a depth of 955.8 m below sea-floor (mbsf, Supplementary Fig. S1b), of which only the bottom 244.5 m was cored.

The upper section of the core comprises a ~40 m-thick poorly sorted sedimentary breccia (Units IVA and IVB) that transitions to a tectonic breccia at ~885 mbsf (Unit IVC and Subunit 1A). The sedimentary breccia contains angular clasts (1–20 cm) of foliated amphibolite, metagabbro, and meta-anorthosite within chalk (Unit IVA) and calcareous mud (Unit IVB). Minor clasts include epidosites and metabasic rocks. The upper tectonic breccias (Unit IVC) have similar clasts in a fine-grained matrix of albite, chlorite, and calcite. Subunit 1A recovers the first mantle lithologies, with tectonic breccia containing serpentinized peridotite clasts and chrysotile-rich veins in a chlorite-serpentine matrix, indicating greenschist- to subgreenschist-facies formation.

Mantle lithologies, cored from 904.2 mbsf to the bottom, yielded 42% recovery (Subunit 1B, cores 22R to 29R; Whitmarsh *et al.*, 1998). These consist of veined, serpentinized peridotites, with foliation intensifying toward the base (173-1068A-25R downward), mainly plagioclase- and spinel-bearing lherzolites intersected by narrow dunite bands. Two highly serpentinized plagioclase lherzolites from cores 27R and 29R (Subunit 1B) were selected for this study (Table 1).

Hole 899B

Hole 899B is located on a basement high, ~ 60 km west of Hole 1068A (Supplementary Fig. S 1c). The borehole penetrated to a depth of 562.5 mbsf, and was cored from 225.5 mbsf downwards.

Peridotite lithologies were recovered below a thick late Pliocene to Late Cretaceous sedimentary sequence in Unit IV, from 369.9 mbsf downward (Supplementary Fig. S1d;

Sawyer *et al.*, 1994). Unit IV A (95 m thick, ~40% recovery) comprises a poorly sorted, polymict serpentinite breccia with interbedded sediments, plus sections of massive serpentinite, serpentinized peridotite, gabbro, and basalt. Most serpentinized peridotite occurs as angular clasts of varying composition, with occasional clasts of mafic metamorphosed rocks. Downhole, Unit IV B (recovery ~14%) contains a 19-m-thick transitional zone of serpentinite breccias, basaltic lavas, and sediments, followed by ~78 m of massive peridotite boulders interbedded with siltstone, basaltic lavas, microgabbros, and mafic rocks. Mafic rocks (basalts, diabases and microgabbros) bearing E-MORB and alkaline affinities (Cornen *et al.*, 1996; Seifert *et al.*, 1997) were found in close association with sedimentary lithologies in Unit IV.

Subunit IVA was interpreted as mass flow generated by submarine slope failure on a fault surface (Comas *et al.*, 1996 and Gibson *et al.*, 1996), and Subunit IVB was interpreted as a Campanian/Maastrichtian mass flow deposit (see Manatschal *et al.*, 2001 and references therein).

Three clasts of harzburgite recovered by Cores 20R, 21R and 22R (Subunit IVA) were selected for this study (Table 1). Of the three investigated Hole 899B peridotites, two (899-3 and 899-4) are spinel harzburgites containing ~ 2-3 vol. % clinopyroxene, and one (899-1) is a plagioclase-bearing harzburgite with clinopyroxene content of ~ 8 vol. %.

Hole 1070A

Hole 1070A is the westernmost WIM borehole where peridotites were recovered (Supplementary Fig. S1e). It lies over an elongated basement ridge, ~ 30 km east of J anomaly, a strong linear magnetic anomaly whose origin was related to the onset of seafloor spreading at ~ 124-127 Ma (Whitmarsh *et al.*, 1998b; Grevemeyer *et al.*, 2022). This basement ridge is parallel to the Iberia continental margin and represents the most oceanward OCT domain sampled in the Iberia Abyssal Plain. The borehole penetrated to a depth of 718.8 mbsf (Supplementary Fig. S1e) and was cored from 599 mbsf downward. The basement (Unit 1 and Unit 2) was encountered at 658.37 mbsf, under a ~ 60 m-thick lower Oligocene to late Aptian sedimentary sequence (Subunit IIC; Units III and IV).

Unit 1 consists of tectonic breccias, similar to Alpine ophicalcites, with poorly sorted, angular to rounded clasts of mostly serpentinized peridotite in a calcite matrix (Manatschal *et al.*, 2001). Rarely, weakly deformed, coarse-grained gabbroic rocks are also found as clasts in the breccia. The contact between Units 1 and 2 is marked by a highly sheared serpentinite (possible fault gauge) over a 2.5-m-thick, locally foliated, pegmatitic gabbros (plagioclase, amphibole, clinopyroxene and ilmenite; Subunit 2a). These gabbros appear to intrude also the underlying serpentinite. Albitite dikelets intruding the serpentinites yield an age of ~ 127 ± 4 Ma (U-Pb ages on zircon, Beard *et al.*, 2002). Similar age constraints (^{39}Ar-^{40}Ar dating = 124.2 ± 0.7 Ma) were obtained by Jagoutz *et al.* (2007) on kaersutitic horneblende. The origin of the pegmatite gabbros is attributed to crystallization from small volume of enriched hydrous melts.

At the bottom of the hole, Subunit 2B comprises partially (~ 75-90%) serpentinized peridotite (core recovery of 39.2%). The coarse-grained peridotite, locally intruded by altered gabbro dikes, is undeformed to weakly foliated, except for a few cores and sections (core 11R, Sections 13R-2, 13R-3, 13R-4, and 14R-3, see Whitmarsh *et al.*, 1998b). Most of the recovered peridotites are lherzolite and harzburgite, but intrusive pyroxenite and dunite were also sampled (Hébert *et al.*, 2001). Four variously serpentinized harzburgites were selected from Subunit 2B (Cores 10R, 12R and 13R, see Table 1).

ANALYTICAL METHODS

Major element mineral compositions were obtained using the Electron Probe MicroAnalyzer (EPMA) JEOL JXA8200 Super Probe operating at the University of Milan (Italy). An accelerating voltage of 15 kV was applied for all analyses. All minerals were measured with a beam current of 15 nA and 1 μm beam size. Counting time was 30 s for peak and 10 s for background.

Minerals trace element compositions were determined at Géosciences Montpellier (AETE-ISO facility, Montpellier University) and at the Geochemistry, Geochronology and Isotope Geology laboratory of the Earth Sciences Department "A. Desio" (University of Milan). At Géosciences Montpellier we used a Thermo Scientific Element 2XR (eXtended Range) high resolution Inductively Coupled Plasma Mass Spectrometer (ICP-MS). The ICP-MS is coupled with laser ablation (LA) system, a Microlas (Geolas Q +) automated platform with a 193 nm Excimer Compex 102 laser from LambdaPhysik. The laser energy density was set to 5 J/cm^2 and ablation frequency to 8 Hz. The laser spot size was set at 110 μm for all the analysed samples, excepted for peridotite 1068-2, for which a spot size of 85 μm was used. At the University of Milan trace elements were analysed by a Laser Ablation ICP-MS instrument consisting of a 193 nm ArF excimer laser equipped with a HelEx 2 volume sample chamber (Analyte Excite – Teledyne – Photon Machines) and a quadrupole ICP-MS (iCAP-Q Thermo Fisher Scientific). Ablation was performed with a spot diameter of 50 μm, a frequency of 10 Hz, and a laser energy of 2 J/cm^2. The data from both laboratories were reduced with the GLITTER software package (Van Achterberg *et al.*, 2001), using the linear fit to ratio method. Data were filtered for spikes on an element-by-element basis. Concentrations were determined against the NIST 612 rhyolitic glass using the values from Pearce et al. (1997), and internal standardization relative to EPMA data was done using ^{29}Si for olivine and orthopyroxene and ^{43}Ca for clinopyroxene. Instrument sensitivity related to analytical conditions was determined from the average across all days of repeat measurements of NIST 612.

Reference basalt BIR-1G was used to monitor accuracy and reproducibility at Géosciences

Montpellier (Supplementary Table S1). For the dataset, reproducibility as constrained by 30 analyses of reference basalt BIR 1-G was better than 5% for most elements except for Li (10%) and for the most depleted elements (<50 ng/g) such as Th and U (10%) and Cs (30%).

Reference basalts ML3B-G and BCR-2G were utilized to assess accuracy and reproducibility at Milan University (Supplementary Table S1). For the dataset, reproducibility and accuracy are better than 2% and 10% for most of the analysed trace elements.

Overall, measured values were comparable within analytical uncertainties to GEOREM accepted values for analyses performed at Géosciences Montpellier and Milan University (Jochum *et al.,* 2005).

SAMPLE DESCRIPTIONS AND PETROGRAPHY

Eight of the selected peridotites are described in detail in this paper (Supplementary Fig. S2). Except for Hole 899B, all the investigated peridotites are extensively serpentinized (serpentinization degree > 80%, see Supplementary Fig. S2), which makes sometimes difficult deciphering primary textural features and initial mineral modes. The main observations and petrographic features of the studied peridotites relevant to this paper are summarized below.

Hole 1068A plagioclase peridotites

The two selected peridotites from Hole 1068A are highly serpentinized (Supplementary Fig. S2 and S3). In thin section, the main textural feature is represented by arrays of mesh serpentine. Serpentine veins ± oxides crosscut the mesh texture and are locally anastomozed, with a variety of morphologies and crosscutting relationships.

Sample 1068-2 preserves clinopyroxene as up to 500 μm in size relics (Fig. 2a and 2b), showing curvilinear boundaries filled by olivine pseudomorphs (Fig. 2b). Orthopyroxene porphyroclasts, up to 1-2 mm sized, are evidenced as bastite pseudomorphs (Fig. 2c). Elongated dark spinel appears invariably mantled by a white to greenish halo composed of very fine-grained, whitish aggregates of chlorite + zoisite + albite after plagioclase (Fig. 2d). These textural features are similar to those observed in plagioclase harzburgite 899-1 (see below), in agreement with the interpretation of Hole 1068A peridotites as plagioclase-bearing peridotites (Whitmarsh *et al.*, 1998b).

By contrast, sample 1068-1 preserves no primary features. Cr-spinel, now completely replaced by magnetite (Supplementary Fig. S3a), shows elongated to holly leaf shapes and is rimmed by whitish coronas of altered plagioclase. These features are akin to Sample 1068-2 and suggest a similar origin.

Hole 899B peridotites

The peridotites are coarse-grained, olivine-rich (~ 70-80 vol.%) granular peridotites preserving evidence of a former spinel-facies foliation, marked by dark elongated spinel.

In the spinel harzburgites, pyroxene porphyroclasts show mostly irregular/curvilinear grain boundaries, with local occurrence of granoblastic domains. Large mantle olivine and pyroxenes display evidence of plastic deformation, as indicated by the diffuse presence of kink bands and undulous extinction. Sub-solidus cooling and re-equilibration is attested by the widespread occurrence of thin exsolution lamellae within pyroxene hosts. Spinel harzburgite samples show microstructures indicating melt-rock reaction, i.e.: (i) crystallization of lobate olivine partly replacing exsolved clino- and orthopyroxene porphyroclasts with irregular outlines (Fig. 3a and 3b); (ii) interstitial (i.e. secondary, ol2) olivine rimming coarse-grained porphyroclastic olivine (Fig. 3c) or orthopyroxene and fine-grained rounded olivine sometimes associated to spinel trails; (iii) small, rounded or interstitial, exsolution-free secondary orthopyroxene (i.e., precipitated from a melt; only in sample 899-4, Fig. 3d).

Clinopyroxene is relatively scarce and tipically occurs as exsolved porphyroclasts, frequently showing evidence of instability, such as corroded rims and irregular outlines (Fig. 3b and 3e).

Brown to dark brown spinel invariably exhibits holly leaf to elongated shape. Spinel trails associated to secondary orthopyroxene were observed in sample 899-4.

Low-temperature alteration phases include small veins of serpentine (± talc), sometimes associated with oxides, and tremolite.

Harzburgite 899-1 is distinguished by the occurrence of plagioclase (~ 3 vol.%), which is completely replaced by low-grade alteration products. This sample shows: (i) secondary orthopyroxene (opx2) + (altered) plagioclase aggregates partially replacing kinked and deformed olivine (Fig. 3f); (ii) (altered) plagioclase rims mantling elongated dark spinel (Fig. 3g). These textures suggest melt interaction with the host peridotite and plagioclase precipitation after percolating melts (melt impregnation). These features are coupled with the occurrence of pyroxene porphyroclasts showing irregular outlines filled by unstrained olivine (Fig. 3h), similar to Hole 899B spinel harzburgites.

Low-temperature alteration phases include small veins of serpentine ± magnetite, crosscutting the rock sample. Tremolitic amphibole was sometimes observed as pyroxene replacement.

Hole 1070A spinel peridotites

Compared to the extensively serpentinized samples of Hole 1068A, slightly lower serpentinization degrees are recorded for Hole 1070A peridotites in thin section, and relict mineral phases are commonly found. Although mantle textures are frequently erased by serpentinization, some distinctive features can be still recognized.

Hole 1070A spinel harzburgites (estimated clinopyroxene content ~ 2-5 vol.%) have coarse-grained granular textures. They show pyroxene-dissolving, olivine-precipitating textures, akin to those displayed by Hole 899B spinel peridotites: (i) porphyroclastic pyroxenes showing jagged, strongly irregular outlines with deep olivine-filled embayments (Fig. 4a); (ii) serpentinized olivine rims mantling bastitic orthopyroxene (Fig. 4b). Clinopyroxene porphyroclasts with tiny extensions propagating among olivine grains and/or along olivine-orthopyroxene contacts (Supplementary Fig. S3b) were also observed. These peculiar propagation textures were previously recognized in some peridotites from the SWIR and were interpreted as resulting from melt-rock reaction (Seyler & Brunelli, 2018).

Olivine is generally replaced by serpentine, with the only exception of sample 1070-4, where fresh and deformed (i.e., kink bands) olivine is easily detected as serpentine mesh cores (Fig. 4c). Fresh olivine is also detected in sample 1070-3. Brown to reddish spinel displays comparatively lower abundances than in other investigated samples. It has holly leaf shapes, sometimes developing tiny extensions and tails like those described for clinopyroxene (Fig. 4d). All samples are optically devoid of plagioclase or cross-cutting magmatic veins.

MINERAL MAJOR ELEMENTS

In situ major element variations of the investigated samples are reported in Supplementary Table S2 and illustrated in Fig. 5, 6 and 7. Overall, our new data only partially overlap with previous literature data, revealing compositions that were not sampled from the previously studied mantle rocks. These new findings, along with the existing literature, confirm and underscore a significant compositional variability for the WIM peridotites. Below, we provide a brief summary of the main compositional features observed in the investigated boreholes.

Hole 1068A

Primary phases were identified only in plagioclase lherzolite 1068-2. Clinopyroxene porphyroclast cores in this sample are enriched in Na_2O (0.61-0.87 wt. %) and Al_2O_3 (5.83-7.10 wt. %), with Cr_2O_3 contents ranging from 0.84 to 1.22 wt. % (Fig. 5). These compositions are akin to refertilized mantle rocks from the SCLM (Picazo *et al.*, 2016). Mg# values (molar (Mg/Mg+Fe(II))) are high and variable, spanning between 0.911-0.943 (Fig. 6a). Compared to other investigated samples, TiO_2 abundances are higher and cover the interval 0.46-0.74 wt. % (Fig. 6b and 6c).

Spinel compositions plot outside the main mantle array (Fig. 7a), displaying lower Mg# values (0.534-0.619) and similar Cr# ((molar (Cr/(Cr+Al)) values (0.255-0.322) compared to peridotites from the other WIM sites. TiO_2 concentrations are comprised between 0.21 and 0.30 wt %. (Fig. 7c).

Hole 899B

Major element chemical variations in Hole 899B are more pronounced than in the other investigated boreholes, with compositions ranging from moderately depleted (spinel harzburgites 899-4 and 899-3) to slightly enriched (plagioclase harzburgite 899-1).

Olivine porphyroclasts in spinel harzburgites 899-3 and 899-4 exhibit variable Fo (Fo= 100 × Mg/(Mg + Fe(II)) in mol%) contents (89.0-91.5, respectively), for NiO ranging between 0.27-0.69 wt. %. Secondary olivine have on average, slightly higher Fo contents (90.5-92.0). Lower Fo contents (89.5-90.0), for NiO contents of 0.16-0.55 wt. %, are observed for plagioclase harzburgite 899-1. Secondary olivine in sample 899-1 spans a wide range of Fo contents (89.9-91.1). CaO is invariably < 0.10 wt. % for all the analyzed samples.

Orthopyroxene has enstatitic composition in all the investigated samples. Mg# of orthopyroxene porphyroclasts varies between 0.900 and 0.918, with the highest and lowest values displayed by sample 899-4 (0.916-0.918) and 899-1 (0.900-0.905), respectively.

Al_2O_3 covers a narrow range of values (2.93-4.43 wt. %), showing decreasing concentrations from porphyroclasts core to rim. Cr_2O_3 ranges between 0.53-0.88 wt. % and exhibits a rough positive correlation with Al_2O_3. CaO ranges between 0.65 and 1.02 wt. %. No significant compositional difference has been detected between orthopyroxene in spinel harzburgites and in the plagioclase-bearing sample. Secondary orthopyroxene in samples 899-1 and 899-4 shows comparatively lower Al_2O_3 (1.67-2.93 wt. %), Cr_2O_3 (0.46-0.70 wt. %) and CaO (0.45-0.77 wt. %) abundances, coupled to higher Mg# values (0.910-0.911 and 0.918-0.920 for sample 899-1 and 899-4 respectively).

Clinopyroxene exhibits a wide spectrum of chemical compositions. Fig. 5 illustrates that porphyroclast cores of Pl-harzburgite 899-1 are more enriched in Na_2O (0.48-0.63 wt. %) and Al_2O_3 (5.37-6.90 wt. %) at comparable Cr_2O_3 contents (1.01-1.32 wt. %) with respect to clinopyroxene of harzburgites 899-3 and 899-4 (Na_2O= 0.23-0.61 wt. %; Al_2O_3 = 4.05-5.25 wt. %; Cr_2O_3= 1.04-1.47 wt. %). For all investigated harzburgites, Na_2O and Al_2O_3 contents decrease from porphyroclast cores to rims to secondary clinopyroxene, where present. Zoning in porphyroclastic clinopyroxene is more pronounced for Al_2O_3, and, in particular, for sample 899-1 (e.g. Al_2O_3 core ~ 5-7 wt. % down to Al_2O_3 rim ~ 3-4 wt. %). Mg# values (Fig. 6a) decrease from spinel harzburgites 899-3 and 899-4 (Mg# 899-3= 0.924-0.937; 899-4= 0.926-0930) to plagioclase harzburgite 899-1 (0.908-0.918). TiO_2 is low (< 0.15 wt. %) and mostly below detection limit for samples 899-3 and 899-4 (Fig. 6b and 6c), in contrast to the higher values displayed by plagioclase harzburgite 899-1 (0.38-0.50 wt. %).

Spinel analyses display a considerable variation in Mg# and Cr# for spinel harzburgites 899-3 and 899-4 (Fig. 7a; Mg#= 0.661-0.785; Cr# = 0.230-0.343), with compositions plotting in the field of abyssal peridotites (Fig. 7a and 7b). TiO_2 is invariably below detection limit (Fig. 7c). In contrast, plagioclase harzburgite 899-1 falls outside the main mantle array (Fig. 7a), displaying lower Mg# (Mg#= 0.512-0.619) and higher Cr# values (Cr#= 0.432-0.463) compared to spinel harzburgites 899-3 and 899-4. TiO_2 contents are high and constant (0.58-0.61 wt. %, Fig. 6c).

Tiny relict patches of fresh plagioclase, rimming spinel porphyroclasts, could be analyzed in sample 899-1. They have Ca-rich compositions (anorthite = An ~ 99 mol%, where An = Ca/(Ca + Na)). Similar anorthite contents were attested in literature for other peridotite samples from Hole 899B (Cornen *et al.*, 1996a). Plagioclase with a lower anorthite content (An ~ 70 mol%) occurs in association with secondary orthopyroxene.

Tremolitic amphibole was detected as low temperature alteration phase in Hole 899B peridotites. It has high Mg# values (0.942-0.955) and low to intermediate Al_2O_3 contents (0.63-3.80 wt. %). TiO_2 is always below detection limit.

Hole 1070A

Olivine was found in samples 1070-3 and 1070-4. It has high and constant Fo contents (91.5-92) and variable NiO abundances (0.21-0.52 wt. %). CaO is < 0.10 wt. % for all the analyzed samples.

Porphyroclastic orthopyroxene has high Mg# (0.915-0.922) and is characterized by Al_2O_3 concentrations (2.62-4.47 wt. %) similar to Hole 899B peridotites, but with higher Cr_2O_3 abundances (0.84-1.12 wt. %). CaO contents vary between 0.56 and 1.08 wt. %.

Clinopyroxene porphyroclasts have distinct major element composition compared to samples from the other boreholes (Fig. 5). They display variable Na_2O (0.41-1.05 wt. %, Fig. 5a), and Al_2O_3 (2.58-5.56 wt. %, Fig. 5b), coupled to high Cr_2O_3 abundances (1.47-2.18 wt. %). Mg# is high and variable (0.921-0.946) and shows a rough negative correlation with Al_2O_3 (Fig. 6a). TiO_2 concentrations are low and comprised between 0.10 and 0.30 wt. % (Fig. 6b and 6c).

Spinel covers a wide range of Mg# and Cr# values (Fig. 7a; Mg#= 0.633-0.745; Cr# = 0.251-0.428), corresponding to slightly to moderately depleted abyssal peridotites. TiO_2 contents are generally below detection limit, apart for sample 1070-4 (TiO_2 = 0.13-0.21 wt. %).

IN SITU GEOCHEMISTRY

Clinopyroxene and orthopyroxene trace element composition

In situ trace element compositions of clino- and orthopyroxene are reported in Supplementary Table S3 and S4 and illustrated in Fig. 8 and 9. Our results show distinct signatures for clinoand orthopyroxenes among the various boreholes, while revealing grain-to-grain and within-grain homogeneity at the sample scale. The main geochemical features of the investigated peridotites of the different boreholes are summarized below.

Hole 1068A

Clinopyroxene exhibits concave downward chondrite-normalized REE patterns (Fig. 8a), yielding gently sloping LREE segments (La_N/Sm_N= 0.22-0.27) and flat HREE (Yb_N= 15-17). Eu negative anomalies are also present. The reported REE patterns overlap in composition with previously analysed plagioclase lherzolites (Abe, 2001). These patterns closely resemble those of clinopyroxene in refertilized mantle rocks from Alpine-Apennine ophiolites (e.g. Kaczmarek & Müntener, 2010; Müntener *et al.*, 2010) .

Primitive mantle (PM)-normalized extended trace element patterns (Fig. 8b) show trace element concentrations ranging between ~ 0.01- 10 PM values. Strong negative anomalies are found for Pb and Sr. LILE (i.e., large ion lithophile element: Cs, Rb, Ba) have low concentrations (< 1 PM) or are below detection limit.

Hole 899B

Chondrite-normalized REE patterns of clino- and orthopyroxene of Hole 899B peridotites reveal a wide range of geochemical signatures, reflecting the lithological and chemical variability of this borehole.

Spinel harzburgites 899-3 and 899-4 (Fig. 8c) have clinopyroxene with V-shaped patterns (La_N/Sm_N= 2.7-3.4), in which the minimum is situated in correspondence of Eu. HREE are strongly fractionated (Dy_N/Yb_N= 0.5-0.6). Spinel harzburgites 899-3 and 899-4 have nearly identical concentrations and fractionations and are distinguished by their HREE concentrations (Yb_N= 2 to 6). PM-normalized extended trace element patterns of spinel harzburgites 899-3 and 899-4 (Fig. 8d) range between 0.03-2 PM values, with no significant spikes. These patterns are uncommon in modern oceans and in the ophiolitic record, while they were testified in mantle xenoliths from central and east Europe (Downes, 2001, 2003; Ionov *et al.*, 2002; Dobosi *et al.*, 2010).

In contrast, plagioclase-bearing harzburgite 899-1 (Fig. 8e) exhibits concave downward chondrite-normalized REE patterns showing with LREE depletion (La_N/Sm_N= 0.02-0.03) and HREE contents higher than abyssal peridotites (Yb_N = 15-17). Eu negative anomalies were also detected. It has trace element concentrations ranging between ~ 0.01- 10 x PM values, with pronounced negative spikes at Pb and Sr, and small negative Zr anomalies (Fig. 8f). LILE have low concentrations (< 0.1 PM). These patterns are common in clinopyroxene of mantle rocks from modern oceans and ophiolites (e.g. Tartarotti *et al.*, 2002; Tribuzio *et al.*, 2004; Rampone *et al.*, 2008).

Orthopyroxene of spinel harzburgites 899-3 and 899-4 (Fig. 9a) have low REE concentrations (~ 0.03-2 chondritic values), similar to the most depleted Mid-Atlantic Ridge abyssal peridotites (i.e., 15°20' Fracture Zone, MAR; e.g. Seyler *et al.*, 2007; Godard *et al.*, 2008; Secchiari, unpubl.). They bear spoon-shaped patterns, with flat to gently sloping LREE-MREE segments (La_N/Sm_N= 0.74-2.85) and steeply plunging HREE (Dy_N/Yb_N= 0.14-0.24). By contrast, the plagioclase harzburgite 899-1 has orthopyroxene patterns (Fig. 9c) displaying REE patterns characterized by steep slopes (Ce_N/Yb_N= 0.004-0.008) and Eu negative anomalies.

PM-normalized extended trace element patterns for the spinel harzburgites 899-3 and 899-4 (Fig. 9b) exhibit low abundances for the most incompatible elements (i.e., LILE: ~ 0.001-0.5 x PM values), with Pb being mostly below the detection limit. Positive spikes are observed for Sr and Ti. Zr and Hf are fractionated (Zr_N/Hf_N = 1.1-1.9). Orthopyroxene of the plagioclase-bearing sample 899-1 (Fig. 9d) is characterized by similar depletion in the most incompatible elements (i.e., Cs, Rb, Ba), while mirroring the most compatible element patterns at higher concentration values. Zr is fractionated compared to Hf (Zr_N/Hf_N = 0.4-0.6).

For all the examined samples from Hole 899B, core to rim variations were not observed.

Hole 1070A

Clinopyroxene in Hole 1070A spinel harzburgites (Fig. 8g) exhibits chondrite-normalized hump-shaped REE patterns (Sm_N/Yb_N= 1.4-2.2), with variably depleted LREE segments (La_N/Nd_N= 0.003-0.146) and low Yb_N (2-6). Similar patterns, although rare in the oceanic mantle, have been reported for some peridotites from slow to ultra-slow ridge segments (e.g. Hellebrand *et al.*, 2002; Seyler *et al.*, 2011).

PM-normalized extended trace element patterns (Fig. 8h) indicate low trace element concentrations, ranging between 0.01- 5 x PM values. Small negative anomalies are observed for Sr. Zr appear slightly fractionated compared to Hf (Zr_N/Hf_N= 0.8-1.2). LILE and Pb are generally below detection limit or strongly depleted (< 1 PM).

Orthopyroxene yields similar hump-shaped chondrite-normalized REE patterns (Fig. 9e), with variably depleted LREE segments (La_N/Sm_N= 0.003-0.16) and gently to steeply sloping HREE segments (Dy_N/Yb_N= 0.42-1.37) for Yb_N= 1-2.

PM-normalized extended trace element patterns (Fig. 9f) show low trace element concentrations (< 1 x PM values), with the most incompatible elements (i.e., LILE, Th, U and Pb) being often below the detection limit. Negative Sr anomalies are detected for all the studied samples. Zr is fractionated compared to Hf (Zr_N/Hf_N = 0.7-1.4).

Olivine trace element composition

Olivine trace element compositions were analyzed in five samples: three from Hole 899B and two from Hole 1070A. Trace element concentrations and REE patterns are reported in Supplementary Table S5 and plotted in Supplementary Fig. S4.

Olivine has similar REE patterns in all the studied samples, with Yb_N ranging from 0.01 to 0.10 (highest Yb_N=0.04-0.10 shown by plagioclase-bearing harzburgite 899-1). These concentrations are in the range of those previously reported for oceanic peridotites (D'Errico *et al.*, 2016). In contrast, MREE and LREE are below detection limit or strongly depleted (Dy_N= 0.002-0.012).

Olivine in spinel peridotites exhibits lower Ti and Y (Ti= 2-12 μg/g; Y= 0.003-0.01 μg/g) compared to sample 899-1 (Ti= 19-26 μg/g; Y= 0.022-0.048 μg/g). Zr is invariably below detection limit for all the analyzed samples.

THERMOBAROMETRY

Equilibrium temperatures calculated for the studied peridotites are reported in Table 6 in Electronic Supplementary material. To investigate the thermal evolution across different temperature intervals (i.e., high and low temperature history), various geothermometers calibrated over elements with different diffusivities were applied. Specifically, we employed: (a) REE-in-two-pyroxene thermometer (Liang *et al.*, (2013); (b) two-pyroxene solvus thermometer (Brey & Köhler, 1990); (c) cation exchange thermometers, i.e., Ca-in-orthopyroxene, olivine-spinel and Ca-in-olivine thermometers (Brey & Kohler, 1990; De Hoog *et al.*, 2010; Li *et al.*, 1995).

For temperature calculations, we considered that only the average compositions of the mineral cores were representative of the initial thermal conditions of the peridotites at depth. The observed core-to-rim variations in major element most likely reflect sub-solidus re-equilibration due to decreasing pressure and temperature during mantle exhumation. This effect has been well-documented for major elements in mantle rocks from fossil OCTs (e.g. Rampone *et al.*, 2005; Montanini *et al.*, 2006; Ferrari *et al.*, 2022). In contrast, the lack of REE zoning can be attributed to their lower diffusivities compared to the fast-diffusing major element.

For temperature calculations, pressure was set at 10 kbar. For sample 899-1, preservation of tiny relics of fresh plagioclase allowed the application of FACE geobarometer (Fumagalli *et al.*, 2017), which yielded a pressure of 5.2 kbar. This value was used for secondary orthopyroxene and porphyroclasts rims of sample 899-1, assuming that equilibration took place in the plagioclase stability field.

REE-in-two-pyroxene thermometer (T_{REE-Y}) applied to Hole 899B and 1070A spinel harzburgites showing Opx-Cpx equilibrium (Supplementary Fig. S5) provides temperature estimates ranging between 1098 °C and 1244 °C, with the highest value shown by spinel harzburgites 1070-2, 1070-3 and 899-4. Plagioclase-bearing harzburgite 899-1 yields T_{REE-Y} = 1168 °C.

Lower temperature values were obtained using the two-pyroxene solvus thermometer (T_{BKN}: Hole 899B samples = 1003-1048 °C; Hole 1070A = 873-984 °C).

Application of Ca-in-orthopyroxene thermometer ($T_{Ca-in-Opx}$) results in temperatures for orthopyroxene cores of Hole 899B peridotites ranging between 985°C and 1029 °C. Cooling of ~ 70-80°C is attested by orthopyroxene rims. Temperatures calculated for the secondary orthopyroxene are shifted towards lower values ($T_{Ca-in-Opx}$= 869-923 °C). For Hole 1070A peridotites, the high serpentinization degree and limited textural control only allowed the application of Ca-in-orthopyroxene thermometer using average orthopyroxene major element composition, which yielded temperatures of 921-972 °C.

Ca-in-olivine and olivine-spinel thermometers calculated for the porphyroclastic assemblages of Hole 899B peridotites provide the lowest temperatures ($T_{Ca-in-Ol}$ = 855-873°C; T_{Ol-Sp} = 770-795°C). These low values possibly indicate significant cooling and re-equilibration over long time intervals. Slightly higher T values ($T_{Ca-in-Ol}$ = 911-937°C; T_{Ol-Sp} = 888-813°C) are provided by Hole 1070A harzburgites. These higher values indicate faster cooling rates compared with Hole 899B samples.

As a whole, temperatures calculated using fast diffusing thermometers are significantly lower than abyssal mantle, and fall in the range of mantle rocks from fossil passive margins (e.g. Rampone *et al.*, 1995; Guarnieri *et al.*, 2012; Ferrari *et al.*, 2022).

Calculated T_{REE-Y} were plotted against T_{BKN}, $T_{Ca-in-Opx}$, T_{Ol-Spl} (Fig. 10). In the variation diagrams, the samples invariably plot above the 1:1 line, partially overlapping the field of hottest ophiolitic peridotites. These features suggest derivation from a mantle section re-heated and variably modified by interaction with percolating melts, followed by relatively slow re-equilibration at lower temperatures, as attested by the temperatures provided by fast diffusing thermometers.

DISCUSSION

The examined samples reveal highly variable mineral modes, textures and chemistries, characterizing the mantle exhumed in the OCT of the WIM. Such variability is observed both within peridotites of the same borehole and among different drill sites. This heterogeneity cannot be attributed to varying degrees of melt extraction of a uniform mantle source occurring at different depths, namely in the spinel or in the garnet stability field (Fig. 11a-b).

We will show that the broad spectrum of petrological and geochemical characters of these mantle domains, along with their atypical distribution compared to hyper-extended margins models (e.g. Picazo *et al.*, 2016) result from interplay between melt-rock interactions –primarily associated to recent rifting processes– and pre-existing mantle heterogeneities. In the following sections, in situ major and trace element data, combined with detailed petrographic analyses, will be used to shed light on the origin and the significance of the different mantle domains.

Hole 1068A plagioclase lherzolites: Melt/rock interactions with MORB-type melts

Plagioclase develops in peridotites either due to sub-solidus decompression from spinel- to plagioclase-facies conditions, often as rims around spinels (Borghini *et al.*, 2010), or as a consequence of melt/rock reactions occurring when peridotites are infiltrated by melts in the plagioclase stability field ("melt impregnation"; e.g. Boudier & Nicolas, 1995; Rampone *et al.*, 1997). "Impregnation" microtextures were widely documented in abyssal and ophiolitic plagioclase peridotites (e.g Tartarotti *et al.*, 2002; Paquet *et al.*, 2016; Rampone *et al.*, 2020 and references therein).

Despite pervasive serpentinization, Hole 1068A plagioclase peridotites provide compelling evidence that plagioclase formed through such a melt/rock process rather than having a sub-solidus origin (e.g. Abe, 2001).

Hole 1068A plagioclase lherzolites 1068-1 and 1068-2 are characterized by (i) deformed dark spinel surrounded by altered plagioclase rims (Supplementary Fig. S2d and S2a) and (ii) clinopyroxene porphyroclasts having corroded rims and outlines (Fig. 2a and 2b). The latter suggests interactions with an infiltrating melt. Primary minerals measured in lherzolite 1068-2, the only sample from Hole 1068A preserving relicts of these minerals, have compositions typically interpreted as evidence of melt-rock interactions: (1) spinels plotting outside the partial melting trend defined by the Cr#–Mg# mantle array (Fig. 7a) with elevated TiO_2 contents (> 0.20 wt. %, Fig. 7c) (e.g., Kelemen *et al.*, 1995; Kaczmarek & Müntener, 2008; Seyler & Bonatti, 1997), (2) clinopyroxenes with Na_2O- and Al_2O_3-rich compositions and marked core-rim zoning similar to SCLM plagioclase peridotites (e.g. Piccardo *et al.*, 2007; Picazo *et al.*, 2016; Rampone *et al.*, 2020), and (3) chondrite-normalized REE patterns bearing high $HREE_N$ and negative Eu anomalies (Fig. 8a), coupled to high Zr/Sr ratios (Fig. 12) suggesting co-precipitation/re-equilibration with plagioclase (Müntener *et al.*, 2010).

To gain further insights into these melt/rock reaction processes, we performed geochemical modelling based on clinopyroxene REE composition. Modelling these reactive processes involves many critical variables, including the composition of the initial mantle source and infiltrating melt, and melt-rock ratio. Aware of the oversimplification inherent in the adopted assumptions, we simulated melt-peridotite interaction using a melt entrapment model in a residual spinel-bearing peridotite, followed by recrystallization and equilibrium trace element redistribution in the plagioclase stability field. By varying the mode of plagioclase peridotite and the composition of the infiltrating liquids, we attempted to match clinopyroxene REE contents of the investigated sample. Details on the model are reported in Supplementary Table S7 and results are illustrated in Fig. 13a. Given that all spinel peridotites analyzed in this study have been variably affected by melt-rock interaction (see next paragraphs), selecting the initial source composition represents a challenging task. For the starting mantle source, we selected a residual peridotite derived from 9% near-fractional melting of a depleted mantle source for 5% melting in the garnet stability field followed by 4% melting in the spinel field. This composition roughly corresponds to the HREE contents and fractionations displayed by spinel harzburgite 899-3. For this sample, the HREE compositions were likely minimally affected by melt-rock interactions, thus representing a reasonable approximation for our calculation. For the infiltrating melt composition, we used the composition of a MORB-like melt from the work of Desmurs *et al.* (2002). Our simple calculation shows that addition of approximately 8% of melt to the starting mantle source composition successfully replicates the clinopyroxene REE patterns observed in sample 1068-2 (Fig. 13a).

Despite its magma-poor nature, samples recovered from dredges and drill holes in the WIM have revealed igneous products with a broad spectrum of geochemical signatures, ranging from MORB-like to geochemically enriched compositions (Seifert & Brunotte, 1996; Seifert *et al.*, 1997; Chazot *et al.*, 2005). Specifically, igneous rocks with MORB-like geochemical fingerprint have been documented in the IAP and Galicia Bank. These melts are thought to originate by melting of a DMM mantle source during the early stages of Mesozoic rifting (e.g. Cornen *et al.*, 1999; Chazot *et al.*, 2006). During that phase, thinning and uplifting of a heterogeneous SCLM was accompanied by the production of small volumes of asthenospheric melts with tholeiitic to transitional compositions (Cornen *et al.*, 1996, 1999; Seifert *et al.*, 1996, 1997). However, the timing of this process remains poorly constrained, particularly in the IAP. The only indirect constraints at Site 1068 come from Ar–Ar cooling ages of ~ 136–137 Ma, obtained from plagioclase in meta-gabbros and a tonalite dyke, which intruded lower to middle crustal meta-amphibolites overlying the exhumed mantle at Hobby High. These ages were interpreted to mark the cooling of these rocks below approximately 200°C during their exhumation to the seafloor, together with the underlying mantle (Féraud *et al.*, 1996), providing a minimum age for magma emplacement in the thinned, hyper-extended crust. Remarkably, at

Site 1068, mantle rocks are found directly beneath the thinned continental crust (Whitmarsh *et al.*, 1998).

The high degree of serpentinization of Hole 1068A samples prevents the application of the FACE geobarometer (Fumagalli *et al.*, 2017) to estimate the pressure related to the refertilization event. However, the pressure value of 5.2 kbar, derived for the plagioclase-bearing harzburgite 899-1, can be reasonably extrapolated to Hole 1068A. This estimate suggests that hot mantle ascended to relatively shallow depths, directly supporting earlier speculations based on geodynamic reconstructions of the West Iberia-Newfoundland conjugate margins (Péron-Pinvidic *et al.*, 2007; Péron-Pinvidic & Manatschal, 2009).

We conclude that the composition of Hole 1068A peridotites reflects the addition of a basaltic MORB-like component to a refractory mantle source. The signature of this mantle domain indicates extensive melt-rock interaction with early rifting-related magmas within a previously depleted, pre-rift mantle source.

Petrological and geochemical constraints on the origin of the Hole 899B harzburgites

Hole 899B peridotites exhibit significant petrological and geochemical variability, offering valuable insights into the nature and history of mantle basement in modern OCTs. In this borehole, variably depleted spinel harzburgites yielding atypical chondrite-normalized V-shaped clinopyroxene REE patterns appear closely associated to LREE-depleted plagioclase harzburgites. In the next paragraphs, the main petrological and geochemical features of these rock types will be assessed to shed light on the origin of Hole 899B peridotites.

Hole 899B spinel harzburgites: ancient SCLM relics or rifting-related evolution?

The overall mineral chemistry of Hole 899B spinel harzburgites – characterized by high Mg# and Cr_2O_3 contents, low Na_2O and TiO_2 in clinopyroxene, and moderate spinel Cr#, (Fig. 5, 6 and 7) – along with the low clinopyroxene modal abundances, suggests that these peridotites represent residues after moderate degrees of melt extraction. Using the calibration of Hellebrand *et al.*, (2001) based on spinel Cr#, the degree of partial melting for samples 899-3 and 899-4 is estimated to range between 9% and 13%, respectively. These estimates are consistent with those derived from clinopyroxene HREE contents (Fig. 14) using the method of Norman (1998). However, when examining REE ratios and HFSE variations (Fig. 11 and 15), the studied lithologies show remarkable deviations from the melting trends. This suggests that the geochemical signature of the analyzed samples has been variably modified by melt-rock reaction, meaning that the investigated peridotites cannot be considered pure partial melting residues.

Evidence of melt-rock interactions is also supported by the microtextural features of these samples, including: (i) secondary olivine precipitation filling irregular grain boundaries and rimming mantle porphyroclasts (i.e. porphyroclastic olivine and pyroxenes); (ii) crystallization of small interstitial secondary orthopyroxene (sample 899-4); and (iii) significantly high (~ 70-80 vol.%) olivine modal abundances. These olivine-enrichment features are typically evidenced in the shallow mantle percolated by deep ascending melts, undersaturated in silica, result in pyroxene dissolution, leading to the formation of olivine-rich "reactive harzburgites" and, ultimately, dunite channels (Kelemen *et al.*, 1990). Such features are found along fossil passive margins (Rampone *et al.*, 2020 and references therein), orogenic massifs and ophiolites (Kelemen *et al.*, 1990) and modern oceanic lithosphere (Tommasi *et al.*, 2004; Niu, 2004; Seyler *et al.*, 2007).

The slightly different mineral major element compositions of harzburgites 899-3 and 899-4 (Fig. 5, 6 and 7), along with their clinopyroxene REE patterns showing sub-parallel HREE segments (Yb_N= 2-6, see Fig. 8) can be either explained by (i) derivation from different mantle sources, (ii) variations in the degree of partial melting linked to different melting depths, or (iii) local variations in the protolith mineralogy. Considering their relative location in the drill core, particularly their proximity (Table 1), it is unlikely that these two samples derive from different mantle sources. In contrast, we favor the interpretation that these harzburgites represent local variations in the protolith mineralogy.

In this framework, the same LREE compositions of sample 899-3 and 899-4 contrasting with their distinct HREE signatures (Fig. 8) can be explained by “chromatographic” chemical re-equilibration during melt percolation (e.g. Navon & Stolper, 1987; Godard *et al.*, 1995).

Despite the complexity introduced by matrix inhomogeneity and the transient nature of trace element exchange processes during melt percolation, an attempt to estimate the composition of the infiltrating melt was made for the harzburgites 899-3 and 899-4 assuming that the peridotites were equilibrated for LREE. The melt in equilibrium with clinopyroxene has LREE-enriched patterns (La_N = 100, Fig. 16) suggesting a role of an enriched melt in the evolution of Hole 899B spinel harzburgites.

Based on our findings, we propose that the main petrological and geochemical characteristics of Hole 899B spinel harzburgites point to a polyphase evolution involving melt depletion followed by melt-rock interaction with enriched melts. However, the geodynamic context of the WIM precludes the hypothesis that such moderate degrees of melt extraction occurred during the recent rifting phase.

In the WIM, continental thinning and breakup led to mantle exhumation across a ~ 160-km-wide region. The low magma productivity (Cornen et al., 1996b) was attributed either to very slow rifting rates (Pérez-Gussinyé *et al.*, 2006), pre-depletion of the asthenosphere following earlier melting events (Müntener & Manatschal, 2006), or exhumation of cold sub-lithospheric mantle (Reston & Morgan, 2004). Therefore, the moderate degrees of melting recorded by these harzburgites likely predate the Late Triassic-Early Cretaceous rifting.

Two different interpretations can be put forward to explain the origin and evolution of Hole 899B spinel harzburgites:

1) Ancient SCLM relics: Hole 899B spinel harzburgites may provide a record of the SCLM predating the rifting event, which likely acquired their geochemical signature during the Variscan orogeny or even earlier. Their distinctive geochemical features, including the rare V-shaped REE patterns in clinopyroxene — only found in mantle xenoliths — suggest that these samples are relics of inherited mantle, unmodified by more recent rifting processes.

2) Partial melting residues modified by rifting: Alternatively, the spinel harzburgites may represent residual SCLM involved in the Mesozoic rifting, modified through melt-rock reaction with enriched melts. Despite the low magma productivity, volcanic rocks with enriched signatures have been identified in the WIM. Notably, basaltic rocks drilled at Hole 899B show enriched signatures, ranging from E-MORB to alkaline (Cornen *et al.*, 1996b; Seifert *et al.*, 1997). These basalts have been interpreted either as syn-rift magmas (Seifert *et al.*, 1997) or as products of seafloor spreading that were nearly contemporaneous with those recovered in Hole 1070A (Beard *et al.*, 2002), marking the onset of oceanic accretion (Péron-Pinvidic *et al.*, 2007). Moreover, strongly enriched alkaline lavas (La_N ~ 100) have been dredged from the Galicia Bank (Chazot *et al.*, 2005), where their emplacement is thought to have occurred during the later stages of high-temperature peridotite deformation at the end of rifting (Malod *et al.*, 1993).

   As a whole, the origin of these enriched signatures has been attributed to mixing between N-MORB and OIB mantle sources (Cornen *et al.*, 1999) or to a contribution from pyroxenite melting (Chazot *et al.*, 2005).

Plagioclase harzburgite 899-1: melt impregnation operated by depleted melts

Plagioclase harzburgite 899-1 was recovered in Hole 899B together with spinel peridotites 899-3 and 899-4. Multiple lines of evidence, similar to those outlined for Hole 1068 peridotites, indicate that plagioclase in sample 899-1 resulted from a melt impregnation reaction. These include: (i) spinel compositional variations, specifically Mg#-Cr# values deviating from the mantle array (Fig. 7a), along with high spinel TiO_2 contents (up to 0.6 wt.%); (ii) elevated Na_2O and Al_2O_3 abundances in clinopyroxene, showing notable core-rim zoning; (iii) high Zr/Sr ratios in clinopyroxene (Fig. 11) associated with $HREE_N$ contents higher than those reported for residual abyssal peridotites.

Melt-rock interaction in sample 899-1 is further testified by the development of distinctive microstructures, such as: (i) the dissolution and replacement of porphyroclastic pyroxene by olivine (Fig. 3h), followed by (ii) the widespread crystallization of secondary orthopyroxene ± (altered) plagioclase aggregates formed at the expenses of olivine porphyroclasts (Fig. 3f) and altered plagioclase rims surrounding spinel elongated along the foliation. These features indicate that the investigated sample records an initial phase of reactive percolation in the spinel stability field, overprinted by reactive melt percolation at shallower depths, i.e. in the plagioclase stability field. To provide more insights into the late melt infiltration event, we have conducted geochemical modelling based on clinopyroxene REE composition. Like previously presented for Hole 1068A plagioclase peridotites, our model calculates the composition of a reacted clinopyroxene by simulating melt-peridotite interaction and subsequent trace element redistribution in the plagioclase stability field. Details on the model are reported in Supplementary Table S7 and results are plotted in Fig. 13b. Our calculation shows that the LREE-depleted chondrite-normalized REE patterns of sample 899-1 can be accounted only considering interaction with a strongly LREE-fractionated melt, more depleted than a typical MORB.

The occurrence of depleted melts has never been documented in the lithological record of the WIM and, in general, has been rarely reported in nature (Ferrando *et al.*, 2024). The existence of such melts has been mainly inferred from geochemical composition of clinopyroxene in ophiolitic and, more rarely, abyssal peridotites (Rampone *et al.*, 2020; Sani *et al.*, 2020), with the only direct evidence coming from olivine-hosted melt inclusions (e.g. Sobolev and Shimizu, 1993; Stracke *et al.*, 2019). Aggregation following melt extraction is generally believed to obscure the depleted nature of such melts, buffering the composition of the aggregated liquids toward more enriched signatures prior to eruption. The genesis of depleted melts has been either ascribed to formation as single incremental melt fractions produced by melting a DM-like mantle source (e.g. Dijkstra *et al.*, 2003; Rampone *et al.*, 2008; Brunelli and Seyler, 2010), or as partly aggregated melts from a refractory mantle source (Stracke *et al.*, 2019; Sanfilippo *et al.*, 2019). Based on the available information, the origin of such depleted melts in the WIM is difficult to ascertain.

Na-Cr rich peridotites from Hole 1070A: open-system melting during incipient oceanization

Hole 1070A harzburgites preserve evidence of partial melting and melt-rock interaction processes occurring in the deep melting region. Similar to the other spinel-bearing samples in our dataset, Hole 1070A peridotites are olivine-rich, coarse-granular harzburgites showing low amounts of modal clinopyroxene. In these samples, deep olivine embayments, often developing at the expense of porphyroclastic pyroxenes, together with olivine-precipitating microstructures, provide evidence of the migration and interaction with a silica-undersaturated melt similar to Hole 899B harzburgites. However, the pronounced resorption features displayed by clinopyroxene (Fig. 4a), and, occasionally by spinel (Fig. 4d), are unusual and were not observed in the other studied samples. Similar features have been documented in natural samples (Dick *et al.,* 2002; Seyler & Brunelli, 2018), as well as in high-temperature magmatic experiments (Koepke *et al.*, 2005). Previous studies have attributed these textures to partial melting and melt-rock reactions occurring during the final melting stages (Seyler & Brunelli, 2018) or to partial melting reaction triggered by water-rich fluids (Koepke *et al.*, 2005),

Mineral chemistry offers contrasting insights into the evolution of Hole 1070A peridotites. The correlation of Cr# in clinopyroxene versus Al_2O_3 and Yb (Fig. 17a and b), suggests that Hole 1070A peridotites represent a suite of residual mantle rocks recording variable degrees of melt extraction. Using Hellebrand *et al.* (2001) formulation, Hole 1070A peridotites appear to have undergone varying amounts of melt depletion, ranging between ~ 10% to 16%. However, clinopyroxene Na_2O abundances are elevated relative to the estimated amounts of melt extraction, as also pointed out by the scattered Na_2O versus Yb trends (Fig. 17c). Moreover, the positive correlation observed between Na_2O and Cr_2O_3 (Fig. 5) cannot be ascribed to melt depletion, as these elements exhibit opposite behaviors during partial melting. While melting in the garnet stability field theoretically has the potential to increase Na_2O concentrations in clinopyroxene due to the higher compatibility of Na at higher pressure (Blundy *et al.* 1995), the chondrite-normalized hump-shaped REE patterns cannot be linked solely to melt extraction. This is clearly illustrated by the Yb_N versus $(Sm/Yb)_N$ and $(Ce/Yb)_N$ diagrams (Fig. 11a and b), where Hole 1070A harzburgites display a distinct deviation from the predicted partial melting trends.

Although uncommon in mantle rock, hump-shaped REE patterns, have been documented in Na-Cr-rich abyssal peridotites from the South West Indian Ridge (i.e. SWIR, Seyler *et al.*, 2011), Central Indian Ridge (i.e. CIR, Hellebrand *et al.*, 2002), and the Arctic Ocean (Hellebrand & Snow, 2003). Hellebrand *et al.* (2002) showed that the entrapment and crystallization as clinopyroxene of a small amount of refractory melt into a refractory harzburgite (refertilization) can lead to a significant increase in Sm/Yb and Ce/Yb ratios while maintaining Yb low and almost constant. As this process proceeds, Sm/Yb and Ce/Yb ratios decrease, whereas Yb increases, with the most reacted samples showing the highest Yb content and the lowest Sm/Yb ratio. This effect arose from the very low modal abundance of clinopyroxene (0.1 vol%) relative to orthopyroxene, with the latter being the major phase controlling bulk distribution coefficients. In contrast, Hole 1070A peridotites are harzburgites with significantly higher clinopyroxene contents (up to 5 vol. %) compared to CIR peridotites. Their trend in the $(Sm/Yb)_N$ and $(Ce/Yb)_N$ versus Yb_N diagrams deviate from those predicted by Hellebrand *et al.* (2002), displaying a $(Sm/Yb)_N$ ratio twice for a similar Yb_N (Fig. 11a). Likewise, $(Ce/Yb)_N$ appears higher for all the analyzed samples, with the exception of harzburgite 1070-3, and refertilization with a depleted melt would not be able to explain the elevated Na_2O abundances in clinopyroxenes from Hole 1070A (up to 1.0 wt. %). All these discrepancies suggest that a different melt composition and refertilization mechanism need to be considered.

The interpretation of Hellebrand et al. (2002) was challenged by Brunelli *et al.* (2014), who demonstrated that the hump-shaped REE patterns can be modelled by incremental open-system melting in the spinel stability field with an inflow of enriched melts. Overall, Brunelli *et al.* (2014) demonstrated that the clinopyroxenes resulting from this process are expected to exhibit a simultaneous decrease in HREEs and increase in LREEs, developing crosscutting trends in the $(Sm/Yb)_N$ versus Yb_N compositional space. This is also accompanied by the counterintuitive positive Na-Cr correlations in clinopyroxene (Seyler and Brunelli, 2018) and Cr# increase in spinel (Seyler *et al.*, 2011).

To explore the nature of the infiltrating melt in Hole 1070A harzburgites, we conducted geochemical modelling to simulate melt entrapment in a refractory peridotite matrix. As a starting composition, we used the same protolith composition as in previous calculations. We then modelled refertilization using the equation of Hellebrand *et al.*, (2002) to calculate clinopyroxene composition after trapping variable amounts of melt. Details on the model are reported in Supplementary Table S7. Our results (Fig. 18) show that addition of small fractions (2-5%) of an enriched melt, derived from 3% near-fractional melting of a DMM in the garnet stability field, can produce chondrite-normalized hump-shaped REE patterns as in samples 1070-1 and 1070-2. By contrast, the model fails to reproduce the LREE-depleted pattern observed in sample 1070-3. While the highly LREE-depleted clinopyroxene from sample 1070-3 broadly resembles a pattern generated by near-fractional melting of a DMM source in the spinel stability field, the notable MREE enrichment, with a distinct peak at Sm, along with the high Na_2O contents (Supplementary Table S1) contradict a purely residual origin. The REE patterns of sample 1070-3 could either reflect incomplete LREE re-equilibration during melt-rock interaction with the enriched melt or the onset of re-equilibration with an incoming MORB melt.

Based on our findings, we propose that the contrasting geochemical signature of Hole 1070A peridotites reflects open system melting in the spinel stability field with continuous inflow of an enriched, garnet-derived melt, which enters the system during melting or in the final melting stages.

Hole 1070A peridotites document a complex magmatic evolution which was likely associated with rifting. Notably, the mantle section is in tectonic contact and crosscut by pegmatite gabbros derived from crystallization of an enriched melt, with compositions similar to E-MORB. High Mg# dikelets, interpreted to reflect more primitive compositions, also occur in association with the pegmatite gabbros (Beard *et al.*, 2002). These gabbros provide geochronological constraints of 127± 4 Ma, akin to the age of the magnetic anomalies M1 and M3 (~ 127-129 Ma), traditionally linked to the onset of oceanic accretion (e.g. Whitmarsh & Wallace, 2001).

In this context, we propose that Hole 1070A peridotites represent partial melting residues that record melt-rock interaction in the deep lithospheric mantle during rifting to oceanization transition. This interpretation is consistent with the geodynamic reconstruction proposed by Péron-Pinvidic & Manatschal (2009), who suggested that the peridotite basement drilled in Hole 1070A represent a slice of deep lithospheric mantle, located close to the lithosphere-asthenosphere boundary during the pre-breakup phase.

The similarities observed between Hole 1070A peridotites and other Na-Cr rich peridotites reported in literature suggest that analogous processes may be shared by slow-to-ultraslow spreading ridge segments and the initial phases of oceanization in magma-poor passive margins. In these settings, the relatively cold thermal regime appears to hinder melt extraction and favor the entrapment of small volumes of deep-seated, transient melts within the partially molten peridotite matrix.

Despite these shared processes, it is noteworthy that some equilibrium temperatures derived from cation-exchange thermometers for Hole 1070A peridotites, specifically $T_{Ca\text{-}in\text{-}Opx}$, are in the range of fossil OCTs peridotites, and lower than abyssal peridotites from slow-spreading ridge settings (Fig. 10 and Supplementary Table S6), arguing for a slow (post-melting) cooling after a high-temperature stage testified by $T_{REE\text{-}Y}$ (~ 1210-1220°C). These results may reflect the prolonged phase of extension and igneous activity proposed for Site 1070 (Tucholke *et al.*, 2007; Jagoutz *et al.*, 2007).

In light of our new findings, we interpret Hole 1070A peridotites, which belong to the most oceanward OCT domain sampled in the IAP, as a transitional mantle domain capturing the onset of oceanization, and the ascent of small magma volumes related to the beginning of oceanic accretion.

CONCLUSIONS

In this study, we investigated the nature and origin of mantle rocks exposed along a modern OCT, by conducting a comprehensive petrological and geochemical study of the peridotites from the WIM sampled at ODP Holes 1068A, 899B, and 1070A.

Despite significant serpentinization, our new data provide compelling evidence of the high degree of petrological and geochemical heterogeneity of the WIM mantle. This heterogeneity, previously speculated only through geodynamic reconstructions of the conjugate Iberia-Newfoundland margins, is testified both across different drill sites and within individual boreholes.

By integrating detailed petrographic observations with in situ major and trace element geochemistry, we identified three distinct mantle domains across an east-west transect, from the most continental to the most oceanward drill sites. These domains are characterized by differing, and sometimes contrasting, geochemical signatures that record the various evolutionary stages of the WIM, from rifting to oceanization. Notably, all mantle domains record evidence of melt/rock interactions, occurring at different pressure and temperature conditions, with different sources and compositions for the infiltrating melts, a paradoxical feature for an "amagmatic" system. This compositional variability of the produced melts, highlighted by our new results, reflects the diverse petrological and geochemical characteristics of the WIM mantle rocks and underscores a high degree of source heterogeneity. More in detail, we identified three mantle domains, moving from the continental to the most oceanward drill sites:

i. Plagioclase impregnation domain: corresponding to Hole 1068A peridotites, this domain closely resembles the plagioclase peridotites from SCLM commonly described in the literature on fossil passive margins. This domain records melt infiltration at shallow levels in hyper-extended lithosphere.

ii. Mixed domain with contrasting geochemical signatures: found at Hole 899B, this domain comprises LREE-depleted plagioclase harzburgites in association with refractory spinel harzburgites, exhibiting V-shaped patterns, never attested in oceanic or ophiolitic peridotites. These features are suggestive either of an ancient, inherited SCLM mantle that remained unaffected by Mesozoic rifting, or partial melting residues that subsequently interacted with rifting-related melts.

iii. Transitional mantle domain: represented by Hole 1070A, this domain displays strong similarities with some Na-Cr-rich peridotites from ultra-slow spreading ridges. Its distinctive geochemical signatures, including rare hump-shaped REE patterns, point to a deep lithospheric origin, likely recording processes that occurred during the transition from rifting to oceanization.

Our findings support a SCLM origin for Hole 899B and 1068A peridotites, while those from Hole 1070A exhibit transitional features between sub-continental lithospheric mantle and oceanic mantle *sensu strictu*.

The documented heterogeneity of the WIM mantle stems from a complex interplay between melt extraction, likely predating the rifting evolution, and varied styles of melt-rock interaction, coupled with different melt compositions, during rifting and development of an embryonic oceanic lithosphere. Although precise chronological constraints on the evolution of these peridotites are lacking—possibly indicating events predating the rifting—the plagioclase impregnation event occurred during lithospheric thinning associated with the rifting process.

These new insights provide a significant contribution to our understanding of OCTs, challenging the traditional and oversimplified view that these regions feature a uniform and predictable distribution of mantle domains. Instead, we propose that OCTs are characterized by a complex mosaic of mantle rocks, showing a remarkable diversity of microstructural and compositional features.

We posit that melt-rock interactions represent the primary mechanisms responsible for producing petrological and chemical heterogeneity in OCTs and the upper mantle in general.

ACKNOWLEDGMENTS

The authors are grateful to O. Bruguier (Géosciences Montpellier), G. Sessa and E. Cannaò (University of Milan) and A. Risplendente for their expertise in LA-ICP-MS and EMPA analyses, respectively. We also wish to thank Andrea Comelli for thin section preparation.

Professors Georg Zellmer and Tod Waight are gratefully acknowledged for their editorial handling. This paper benefited of comments of three anonymous reviewers, who significantly improved the initial version of this manuscript.

This research was funded through MUR for ECORD-IODP Italia (grant "ECORD-IODP Italia 2021") awarded to A. Secchiari. This work has also benefited from the equipment and framework of the COMP-HUB and COMP-R Initiatives, funded by the 'Departments of Excellence' program of the Italian Ministry for University and Research (MIUR, 2018-2022 and MUR, 2023-2027).

DATA AVAILABILITY STATEMENT

The data underlying this article are included as supplementary material and are available in GFZ Data Services at [*https://doi.org/10.5880/fidgeo.2024.011*](https://doi.org/10.5880/fidgeo.2024.011).

REFERENCES

Abe, N. (2001). Petrochemistry of serpentinized peridotite from the Iberia Abyssal Plain (ODP Leg 173): its character intermediate between sub-oceanic and sub-continental upper mantle. In: Wilson RCL, Whitmarsh RB, Taylor B, Froitzheim N (eds) Non-Volcanic Rifting of Continental Margins: Evidence from Land and Sea. Geol Soc (London), Spec Publ 187, pp 143–159.

Arai, S. (1994). Characterization of spinel peridotites by olivine-spinel compositional relationships: Review and interpretation. *Chemical Geology* **113**, 191–204.

Beard, J. S., Fullagar, P. D. & Sinha, A. K. (2002). Gabbroic Pegmatite Intrusions , Iberia Abyssal Plain , ODP Leg 173 , Site 1070 : Magmatism during a Transition from Non-volcanic Rifting to Sea-floor Spreading. **43**, 885–905.

Blundy J.D., Falloon, B.J., Wood. J. & Dalton A., 1995. Sodium partitioning between clinopyroxene and silicate melts. *Journal of Geophysical Research: Solid Earth* **100**, 15501-15515.

Boillot, G. *et al*. (1987). Tectonic denudation of the upper mantle along passive margins: a model based on drilling results (ODP leg 103, western Galicia margin, Spain). *Tectonophysics* **132**, 335–342.

Boillot, G., Féraud, G., Recq, M. & Girardeau, J. (1989). Undercrusting by serpentinite beneath rifted margins. *Nature* **341**, 523–525.

Borghini, G., Fumagalli, P., Rampone, E. (2010). The stability of plagioclase in the upper mantle: subsolidus experiments on fertile and depleted lherzolite. *Journal of Petrology*, **51** (1–2), 229-254.

Boudier, F., Nicholas, A. (1995). Nature of the Moho transition zone in the Oman ophiolite. *Journal of Petrology* 36, 777-796.

Brey, G. P. & Köhler, T. (1990). Geothermobarometry in four-phase lherzolites II. New thermobarometers, and practical assessment of existing thermobarometers. *Journal of Petrology* **31**, 1353–1378.

Brunelli, D., Paganelli, E. & Seyler, M. (2014). Percolation of enriched melts during incremental open-system melting in the spinel field: A REE approach to abyssal peridotites from the Southwest Indian Ridge. *Geochimica et Cosmochimica Acta*. Elsevier Ltd **127**, 190–203.

Brunelli, D. & Seyler, M. (2010). Asthenospheric percolation of alkaline melts beneath the St. Paul region (Central Atlantic Ocean). *Earth and Planetary Science Letters* **289**, 393–405.

Charpentier, S., Kornprobst, J., Chazot, G., Cornen, G. & Boillot, G. (1998). Interaction entre lithosphère et asthénosphère au cours de l'ouverture océanique : données isotopiques préliminaires sur la Marge passive de Galice (Atlantique-Nord). *Comptes Rendus de l'Académie des Sciences - Series IIA - Earth and Planetary Science*. Elsevier Masson **326**, 757–762.

Chazot, G., Charpentier, S., Kornprobst, J., Vannucci, R., Luais, B (2005). Lithospheric Mantle Evolution during Continental Break-Up: The West Iberia Non-Volcanic Passive Margin. *Journal of Petrology* **46**, 2527–2568.

Cornen, G., Beslier, M.-O. & Girardeau, J. (1996a). Petrologic Characteristics of the Ultramafic Rocks from the Ocean/Continent Transition in the Iberia Abyssal Plain. *Proceedings of the Ocean Drilling Program, Scientific Results* **149**, 377–395.

Cornen, G., Beslier, M.-O. & Girardeau, J. (1996b). Petrology of the mafic rocks cored in the Iberia Abyssal Plain. *Proceedings of the Ocean Drilling Program, 149 Scientific Results*. Ocean Drilling Program.

Cornen, G., Girardeau, J., Monnier, C., (1999). Basalts, underplated gabbros and pyroxenites record the rifting process of the West Iberian margin. *Mineralogy and Petrology*, **67**, 111-142.

De Hoog, J.C.M., Gall, L., and Cornell, D. H. (2010). Trace-element geochemistry of mantle olivine and application to mantle petrogenesis and geothermobarometry. *Chemical Geology* **270**, 196–215.

Desmurs, L., Müntener, O., Manatschal, G., (2002). Onset of magmatic accretion within a magma-poor rifted margin: a case study from the Platta ocean–continent transition, eastern Switzerland. *Contributions to Mineralogy and Petrology*, **144**:365–382.

D'Errico, M.E., Warren, J.M., Godard, M. (2016). Evidence for chemically heterogeneous Arctic mantle beneath the Gakkel Ridge. *Geochimica et Cosmochimica Acta*, **174**, 291-312.

Dick, H. J. B. and Bullen, T. (1984). Chromian spinel as a petrogenetic indicator in abyssal and alpine-type peridotites and spatially associated lavas. *Contributions to Mineralogy and Petrology* **86**, 54–76.

Dick, H.J.B., Ozawa, K., Meyer, P.S., Niu, Y., Robinson, P.T., Constantin, M. & Hebert, R., Maeda, J., Natland, J.H., Hirth, J.G., Mackie, S. M. (2002). Primary silicate mineral chemistry of a 1.5-km section of very slow spreading lower ocean crust: ODP Hole 735B, Southwest Indian Ridge. *Natland, J.H., Dick, H.J.B., Miller, D.J., Von Herzen, R.P. (Eds.), Proc. ODP, Sci. Results* **176**.

Dijkstra, A. H., D., Sergeev, S., Spandler, C., Pettke, T., Meisel, T., and Cawood, P.A. (2010), Highly refractory peridotites on Macquarie Island and the case for anciently depleted domains in the Earth's mantle, *Journal of Petrology*, **51**(1-), 469–493.

Dobosi, G., Jenner, G. A., Embey-Isztin, A. & Downes, H. (2010). Cryptic metasomatism in clino- and orthopyroxene in the upper mantle beneath the Pannonian region. *Geological Society Special Publication* **337**, 177–194.

Downes, H. (2001). Formation and modification of the shallow sub-continental lithospheric mantle: A review of geochemical evidence from ultramatic xenolith suites and tectonically emplaced ultramafic massifs of Western and Central Europe. *Journal of Petrology* **42**, 233–250.

Downes, H., Beard, A. & Hinton, R. (2004). Natural experimental charges: an ion-microprobe study of trace element distribution coefficients in glass-rich hornblendite and clinopyroxenite xenoliths. *Lithos*. Elsevier **75**, 1–17.

Downes, H., Reichow, M. K., Mason, P. R. D., Beard, A. D. & Thirlwall, M. F. (2003). Mantle domains in the lithosphere beneath the French Massif Central: Trace element and isotopic evidence from mantle clinopyroxenes. *Chemical Geology* **200**, 71–87.

Dygert, N. & Liang, Y. (2015). Temperatures and cooling rates recorded in REE in coexisting pyroxenes in ophiolitic and abyssal peridotites. *Earth and Planetary Science Letters*. Elsevier B.V. **420**, 151–161.

Féraud, G., Beslier, M.-O., and Cornen, G., 1996. 40Ar/39Ar dating of gabbros from the ocean/continent transition of the western Iberia margin: preliminary results. In Whitmarsh, R.B., Sawyer, D.S., Klaus, A., and Masson, D.G. (Eds.), Proc. ODP, Sci. Results, 149: College Station, TX (Ocean Drilling Program), 489–495.

Ferrando, C., Borghini, G., Sani, C., Genske, F., Ligi, M., Stracke, A. & Sanfilippo, A. (2024). Deep segregation and crystallization of ultra-depleted melts in the sub-ridge mantle. *Chemical Geology* **644**, 121840.

Ferrari, E., Montanini, A. & Tribuzio, R. (2022) Rifting evolution of the lithospheric subcontinental mantle: New insights from the External Ligurian ophiolites (Northern Apennine, Italy). Lithos **410-411**, 106571.

Fumagalli, P., Borghini, G., Rampone, E. & Poli, S. (2017). Experimental calibration of Forsterite–Anorthite–Ca-Tschermak–Enstatite (FACE) geobarometer for mantle peridotites. *Contributions to Mineralogy and Petrology* **172**, 38.

Gibson, I.L., Beslier, M.-O., Cornen, G., Milliken, K.L., and Seifert, K.E. (1996). Majorand trace-element seawater alteration profiles in serpentinite formed during the development of the Iberia margin, Site 897. In Whitmarsh, R.B., Sawyer, D.S., Klaus, A., and Masson, D.G. (Eds.), Proc. ODP, Sci. Results, 149: College Station, TX (Ocean Drilling Program), 519–527. doi:10.2973/odp.proc.sr.149.219.1996

Godard, M., Bodinier, J. L. & Vasseur, G., (1995). Effects of mineralogical reactions on trace element redistributions in mantle rocks during percolation processes: a chromatographic approach. *Earth and Planetary Science Letters* **133**, 449–461.

Godard, M., Lagabrielle, Y., Alard, O. & Harvey, J. (2008). Geochemistry of the highly depleted peridotites drilled at ODP Sites 1272 and 1274 (Fifteen-Twenty Fracture Zone, Mid-Atlantic Ridge): Implications for mantle dynamics beneath a slow spreading ridge. *Earth and Planetary Science Letters* **267**, 410–425.

Grevemeyer, I., Ranero, C. R., Papenberg, C., Sallares, V., Bartolomé, R., Prada, M., Batista, L. & Neres, M. (2022). The continent-to-ocean transition in the Iberia Abyssal Plain. *Geology* **50**, 615–619.

Guarnieri, L., Nakamura, E., Piccardo, G. B., Sakaguchi, C., Shimizu, N., Vannucci, R. & Zanetti, a.

(2012). Petrology, Trace Element and Sr, Nd, Hf Isotope Geochemistry of the North Lanzo Peridotite Massif (Western Alps, Italy). *Journal of Petrology* **53**, 2259–2306.

Kelemen, P.B., Joyce, D.B., Webester, J.D. & Holloway, J.R (1990) Reaction between ultramafic rock and fractionating basaltic magma II. Experimental Investigation of Reaction Between Olivine Tholeiite and Harzburgite at 1150–1050°C and 5 kb. *Journal of Petrology* **31,** 99-134.

Kelemen, P.B, Whitehead, J.A., Aharonov, E., Jordahl, K.A. & 1995. Experiments on flow focusing in soluble porous media, with applications to melt extraction from the mantle. *Journal of Geophysical Research* **100**:B1475–96.

Hébert, R., Gueddari, K., Laflèche, M. R., Beslier, M. O. & Gardien, V. (2001). Petrology and geochemistry of exhumed peridotites and gabbros at non-volcanic margins: ODP Leg 173 West Iberia ocean-continent transition zone. *Geological Society Special Publication* **187**, 161–189.

Hellebrand, E. & Snow, J. E. (2003). Deep melting and sodic metasomatism underneath the highly oblique-spreading Lena Trough (Arctic Ocean). *Earth and Planetary Science Letters* **216**, 283–299.

Hellebrand, E., Snow, J. E., Dick, H. J. & Hofmann, a. W. (2001). Coupled major and trace elements as indicators of the extent of melting in mid-ocean-ridge peridotites. *Nature* **410**, 677–681.

Hellebrand, E., Snow, J. E., Hoppe, P. & Hofmann, a W. (2002). Garnet-field melting and late-stage refertilization in “residual” abyssal peridotites from the Central Indian Ridge. *Journal of Petrology* **43**, 2305–2338.

Ionov, D. A., Bodinier, J. L., Mukasa, S. B. & Zanetti, A. (2002). Mechanisms and sources of mantle metasomatism: Major and trace element compositions of peridotite xenoliths from Spitsbergen in the context of numerical modelling. *Journal of Petrology* **43**, 2219–2259.

Ishii, T., Robinson, P. T., Maekawa, H. & Fiske, R. (1992). Petrological studies of peridotites from diapiric serpentinite seamounts in the Izu-Ogasawara-Mariana Forearc, Leg 125. *Proceedings of the Ocean Drilling Program, Scientific Results* **125**, 445–485.

Jagoutz, O., Muntener, O., Manatschal, G., Rubatto, D., Peron-Pinvidic, G., Turrin, B.D. , Villa, I.M. (2007). The rift-to-drift transition in the North Atlantic: a stuttering start of the MORB machine? *Geology*, **35**, 1087-1090.

Li, J., Kornprobst, J., Vielzeuf, D. & Fabriès, J. (1995). An improved experimental calibration of the olivine-spinel geothermometer. *Chinese Journal of Geochemistry*. Science in China Press **14**, 68–77.

Kaczmarek, M. A. & Müntener, O. (2008). Juxtaposition of melt impregnation and high-temperature shear zones in the upper mantle; field and petrological constraints from the lanzo peridotite (Northern Italy). *Journal of Petrology* **49**, 2187–2220.

Koepke, J., Feig, S.T., Snow, J. (2005). Hydrous partial melting within the lower oceanic crust. *Terra Nova*, **17**:286–291.

Liang, Y., Sun, C. & Yao, L. (2013). A REE-in-two-pyroxene thermometer for mafic and ultramafic rocks. *Geochimica et Cosmochimica Acta*. Elsevier Ltd **102**, 246–260.

McCarthy, A., Falloon, T. J., Sauermilch, I., Whittaker, J. M., Niida, K. & Green, D. H. (2020). Revisiting the Australian-Antarctic Ocean-Continent Transition Zone Using Petrological and Geophysical Characterization of Exhumed Subcontinental Mantle. *Geochemistry, Geophysics, Geosystems* **21**.

Mccarthy, A. & Müntener, O. (2019). Evidence for ancient fractional melting , cryptic refertilization and rapid exhumation of Tethyan mantle (Civrari Ophiolite , NW Italy). *Contributions to Mineralogy and Petrology*. Springer Berlin Heidelberg **174**, 1–25.

Minshull, T. A., Dean, S. M. & Whitmarsh, R. B. (2014). The peridotite ridge province in the southern Iberia Abyssal Plain: Seismic constraints revisited. *JGR Solid Earth* **119**, 1580–1598.

Montanini, A., Tribuzio, R. & Anczkiewicz, R. (2006). Exhumation history of a garnet pyroxenite-bearing mantle section from a continent-ocean transition (Northern Apennine Ophiolites, Italy). *Journal of Petrology* **47(10)**, 1943–1971.

Malod, J.A., Murillas, J., Kornprobst, J., Boillot, G. (1993). Oceanic lithosphere at the edge of a Cenozoic active continental margin (northwest slope of Galicia Bank, Spain). *Tectonophysics*, **221**, 195-206

Manatschal, G., Froitzheim, N., Rubenach, M. & Turrin, B. D. (2001). The role of detachment faulting in the formation of an ocean–continent transition: insights from the Iberia Abyssal plain. In: Wilson, R. C. L., Withmarsh, R. B., Taylor, B. & Froitzheim, N. (eds) Non-Volcanic Rifting of Continental Margins: a Comparison of Evidence from Land and Sea. *Geological Society, London, Special Publications* **187**, 405–428.

Manatschal, G. & Müntener, O. (2009). A type sequence across an ancient magma-poor ocean-continent transition: the example of the western Alpine Tethys ophiolites. *Tectonophysics* **473**, 4-19.

Montanini, A., Tribuzio, R., Anczkiewicz, R. (2006). Exhumation history of a garnet pyroxenite-bearing mantle section from a continent-ocean transition (northern Apennine ophiolites, Italy). *Journal of Petrology*, **47** (10) , 1943-1971

Müntener, O., Pettke, T., Desmurs, L., Meier, M. & Schaltegger, U. (2004). Refertilization of mantle peridotite in embryonic ocean basins: trace element and Nd isotopic evidence and implications for crust–mantle relationships. *Earth and Planetary Science Letters* **221**, 293-308.

Müntener, O. & Manatschal, G. (2006). High degrees of melt extraction recorded by spinel harzburgite of the Newfoundland margin: The role of inheritance and consequences for the evolution of the southern North Atlantic. *Earth and Planetary Science Letters* **252**, 437–452.

Müntener, O., Manatschal, G., Desmurs, L. & Pettke, T. (2010). Plagioclase Peridotites in Ocean–Continent Transitions: Refertilized Mantle Domains Generated by Melt Stagnation in the Shallow Mantle Lithosphere. *Journal of Petrology*. Oxford Academic **51**, 255–294.

Norman, M.D. (1998). Melting and metasomatism in the continental lithosphere: laser ablation ICPMS analysis of minerals in spinel lherzolites from eastern Australia. *Contributions to Mineralogy and Petrology*, **130**, 240-255

Navon, O. & Stolper, E. (1987). Geochemical consequences of melt percolation: the upper mantle as a chromatographic column. *journal of geology* **95**, 285–307.

Niu, Y. (2004). Bulk-rock major and trace element compositions of abyssal peridotites: implications for mantle melting, melt extraction and post-melting processes beneath mid-ocean ridges. *Journal of Petrology* **45**, 2423-2458.

Paquet, M., Cannat, M., Brunelli, D., Hamelin, C., Humler, E. (2016). Effect of melt/mantle interactions on MORB chemistry at the easternmost Southwest Indian Ridge (61°–67°E). *Geochemistry Geophysics Geosystems*, 10.1002/2016GC006385.

Pearce, N.J., Perkins, W.T., Westgate, J.A., Gorton, M.P., Jackson, 1028 S.E., Neal, C.R., Chenery, S. P. (1997). A compilation of new and published major and trace element data for NIST SRM 610 and NIST SRM 612 glass reference materials. *Geostandards newsletters* **21**, 115–144.

Pearce, J. a, Barker, P. F., Edwards, S. J., Parkinson, I. J. & Leat, P. T. (2000). Geochemistry and tectonic significance of peridotites from the South Sandwich arc-basin system, South Atlantic. *Contributions to Mineralogy and Petrology* **139**, 36–53.

Pérez-Gussinyé, M., Morgan, J. P., Reston, T. J. & Ranero, C. R. (2006). The rift to drift transition at non-volcanic margins: Insights from numerical modelling. *Earth and Planetary Science Letters*. Elsevier **244**, 458–473.

Péron-Pinvidic, G., Manatschal, G., Minshull, T., Sawyer, D. (2007). Tectonosedimentary evolution of the deep Iberia-Newfoundland margins: evidence for a complex breakup history. *Tectonics*, **26**, TC2001.

Péron-Pinvidic, G., Manatschal, G., (2009). The final rifting evolution at deep magma-poor passive margins from Iberia-Newfoundland: a new point of view. *International Journal of Earth Sciences*, **98**, 1581-1597.

Picazo, S., Müntener, O., Manatschal, G., Bauville, A., Karner, G. & Johnson, C. (2016). Mapping the nature of mantle domains in Western and Central Europe based on clinopyroxene and spinel chemistry: Evidence for mantle modification during an extensional cycle. *Lithos*. Elsevier B.V. **266–267**, 233–263.

Piccardo, G. B., Zanetti, a. & Müntener, O. (2007). Melt/peridotite interaction in the Southern Lanzo peridotite: Field, textural and geochemical evidence. *Lithos* **94**, 181–209.

Rampone, E., Hoffman, A.W., Piccardo, G., Vannucci, R. (1995). Petrology, Mineral and Isotope Geochemistry of the External Liguride Peridotites (Northern Apennines, Italy). *Journal of Petrology* **36**, 81–105.

Rampone, E., Borghini, G. & Basch, V. (2020). Melt migration and melt-rock reaction in the Alpine-Apennine peridotites: Insights on mantle dynamics in extending lithosphere. *Geoscience Frontiers*. Elsevier Ltd **11**, 151–166.

Rampone, E., Hofmann, a. W., Piccardo, G. B., Vannucci, R., Bottazzi, P. & Ottolini, L. (1996). Trace element and isotope geochemistry of depleted peridotites from an N-MORB type ophiolite (Internal Liguride, N. Italy). *Contributions to Mineralogy and Petrology* **123**, 61–76.

Rampone, E., Piccardo, G. B. & Hofmann, A. W. (2008). Multi-stage melt–rock interaction in the Mt.

Maggiore (Corsica, France) ophiolitic peridotites: microstructural and geochemical evidence. *Contributions to Mineralogy and Petrology* **156**, 453–475.

Rampone, E., Romairone, a. & Hofmann, a. W. (2004). Contrasting bulk and mineral chemistry in depleted mantle peridotites: evidence for reactive porous flow. *Earth and Planetary Science Letters* **218**, 491–506.

Rampone, E., Romairone, A., Abouchami, W., Piccardo, G. B. & Hofmann, A. W. (2005). Chronology, petrology and isotope geochemistry of the Erro-Tobbio peridotites (Ligurian Alps, Italy): Records of Late Palaeozoic lithospheric extension. *Journal of Petrology* **46**, 799–827.

Rampone, E., Piccardo, G.B., Vannucci, R., Bottazzi, P. (1997). Chemistry and origin of trapped melts in ophiolitic peridotites. *Geochimica et Cosmochimica Acta*, **61**, 4557-4569.

Reston, T. J. & Morgan, J. P. (2004). Continental geotherm and the evolution of rifted margins. *Geology*. GeoScienceWorld **32**, 133–136.

Sanfilippo, A., Salters, V., Tribuzio, R. & Zanetti, A. (2019). Role of ancient, ultra-depleted mantle in Mid-Ocean-Ridge magmatism. *Earth and Planetary Science Letters*. Elsevier **511**, 89–98.

Sanfilippo, A. & Tribuzio, R. (2011). Melt transport and deformation history in a nonvolcanic ophiolitic section, northern Apennines, Italy: Implications for crustal accretion at slow spreading settings. *Geochemistry, Geophysics, Geosystems* **12**, n/a-n/a.

Sani, C., Sanfilippo, A., Ferrando, C., Peyve, A.A., Skolotonev, S.G., Muccini, F., Zanetti, A., Basch, V., Palmiotto, C., Bonatti, E., Ligi, M. (2020). Ultra-depleted melt refertilization of mantle peridotites in a large intra-transform domain (Doldrums Fracture Zone; 7–8°N, Mid Atlantic Ridge). *Lithos*, **374**, Article 105698.

Sawyer, Dale. S.Whitmarsh, R. B., Klaus, A. & Party, and S. S. (1994). Site 899. *Proceedings of the Ocean Drilling Program, Initial Reports* **149**, 1–63.

Seifert, K. & Brunotte, D. (1996). Geochemistry of serpentinized mantle peridotite from Site 897 in the Iberia Abyssal Plain. *Proceedings of the Ocean Drilling Program, 149 Scientific Results* **149**.

Seifert, K. E., Chang, C.-W. & Brunotte, D. A. (1997). Evidence from Ocean Drilling Program Leg 149 mafic igneous rocks for oceanic crust in the Iberia Abyssal Plain zone Drilling Program transition (OCT) on the Iberia Abyssal Plain and its role in the opening of the Atlantic Ocean approximately rocks recov. **102**, 7915–7928.

Seyler, M. & Bonatti, E. (1997). Regional-scale melt–rock interaction in lherzolitic mantle in the Romanche Fracture Zone (Atlantic Ocean). *Earth and Planetary Science Letters*, **146**, 273-287.

Seyler, M. & Brunelli, D. (2018). Sodium- chromium covariation in residual clinopyroxenes from abyssal peridotites sampled in the 43°–46°E region of the Southwest Indian Ridge. *Lithos*. Elsevier B.V. **302**–**303**, 142–157.

Seyler, M., Brunelli, D., Toplis, M. J. & Mével, C. (2011). Multiscale chemical heterogeneities beneath the eastern Southwest Indian Ridge (52°E-68°E): Trace element compositions of along-axis dredged peridotites. *Geochemistry, Geophysics, Geosystems*. Blackwell Publishing Ltd **12**.

Seyler, M., Lorand, J.-P., Dick, H. J. B. & Drouin, M. (2007). Pervasive melt percolation reactions in ultra-depleted refractory harzburgites at the Mid-Atlantic Ridge, 15° 20′N: ODP Hole 1274A. *Contributions to Mineralogy and Petrology* **153**, 303–319.

Seyler, M., Toplis, M. J., Lorand, J. P., Luguet, a. & Cannat, M. (2001). Clinopyroxene microtextures reveal incompletely extracted melts in abyssal peridotites. *Geology* **29**, 155–158.

Skelton, A.D.L & Valley J.W. (2000). The relative timing of serpentinisation and mantle exhumation at the ocean–continent transition, Iberia: constraints from oxygen isotopes. *Earth and Planetary Science Letters* **178**, 327-338.

Sobolev, A. V. & Shimizu, N. (1993). Ultra-depleted primary melt included in an olivine from the Mid-Atlantic Ridge. *Nature 1993 363:6425*. Nature Publishing Group **363**, 151–154.

Stracke, A., Genske, F., Berndt, J. & Koornneef, J. M. (2019). Ubiquitous ultra-depleted domains in Earth's mantle. *Nature Geoscience 2019 12:10*. Nature Publishing Group **12**, 851–855.

Sun, S. -s. & McDonough, W. F. (1989). Chemical and isotopic systematics of oceanic basalts: implications for mantle composition and processes. *Geological Society, London, Special Publications* **42**, 313–345.

Tartarotti, P., Susini, S., Nimis, P., Ottolini, L. (2002). Melt migration in the upper mantle along the Romanche Fracture Zone (Equatorial Atlantic). *Lithos*, **63**, 125-149.

Taylor & R., W. (1998). An experimental test of some geothermometer andgeobaro-meter formulations for upper mantle peridotites withapplication to the ther-mobarometry of fertile lherzolite and garnetwebsterite. *Neues Jahrbuch für Mineralogie - Abhandlungen*. Schweizerbart'sche Verlagsbuchhandlung 381–408.

Tommasi, A., Godard, M., Coromina, G., Dautria, J.-M. & Barsczus, H.G. (2004). Seismic anisotropy and compositionally induced velocity anomalies in the lithosphere above mantle plumes: a petrological and microstructural study of mantle xenoliths from French Polynesia. *Earth and Planetary Science Letters* **227**, 539-556.

Tribuzio, R., Thirlwall, M. F. & Vannucci, R. (2004). Origin of the Gabbro–Peridotite Association from the Northern Apennine Ophiolites (Italy). *Journal of Petrology*. Oxford Academic **45**, 1109–1124.

Van Achterbergh, E., Ryan, C., Jackson, S., Griffin, W. (2001). Data reduction software for LA-ICP-MS. In: Sylverster P (ed) LaserAblation ICPMS in the Earth Sciences – *Principles and applications, Min Assoc Can Short Course Series*, **29**, 239-243.

Warren, J. M. (2016). Global variations in abyssal peridotite compositions. *Lithos*. Elsevier, 193–219.

Whitmarsh, R. B. & Sawyer, D. S. (1996). The ocean/continent transition beneath the Iberia Abyssal Plain and continental-rifting to seafloor-spreading processes. *Proceedings of the Ocean Drilling Program, 149 Scientific Results* **149**, 713–733.

Whitmarsh, R. B., Beslier, M.-O. & Wallace, P.J., et al. (1998). Site 1070. *Proceedings of the Ocean Drilling Program, Initial Reports* ***173***, 265–294.

Whitmarsh, R. B. & Wallace, P. J. (2001). The rift-to-drift development of the West Iberia non volcanic continental margin: A summary and review of the contribution of ocean drilling program leg 173. In: Beslier, M. O., Whitmarsh, R. B., Wallace, P. J.& Girardeau, J. (eds) *Proceedings of the Ocean*

*Drilling Program, Initial Reports **173***, Ocean Drilling Program, College Station, TX.

Figure captions

Fig. 1. Simplified map of the West Iberian margin (WIM). Thick black line: ultramafic ridge; thick dashed line: J magnetic anomaly. Open squares represent Leg 149 (Site 899) and 173 (Sites 1068 and 1070) drill sites investigated in this study.

Fig. 2. Representative microphotographs of Hole 1068A peridotites: (a) strongly serpentinized porphyroclastic clinopyroxene relic (sample 1068-2, plane polarized light, PPL); (b) relic clinopyroxene showing corroded rims filled by olivine pseudomorphs (cross polarized light, XPL); (c) orthopyroxene porphyroclasts preserved as bastite pseudomorphs (XPL); d) aligned, deformed spinel rimmed by (altered) plagioclase (PPL), note the similarity with sample 899-1 (Fig. 3g).

Fig. 3. Representative microtextural features shown by Hole 899B peridotites. Spinel harzbugites: (a) Large corroded orthopyroxene porphyroclast filled by newly-formed olivine (sample 899-4, XPL); (b) porphyroclastic clinopyroxene showing curvilinear outlines against olivine-orthopyroxene porphyroclasts (sample 899-3, XPL); (c) interstitial olivine (Ol2) developing on olivine porphyroclasts (sample 899-3, XPL); (d) secondary orthopyroxene (Opx2) precipitation on the main porphyroclastic assemblage (sample 899-4, XPL); (e) resorbed interstitial clinopyroxene displaying evidence of instability (sample 899-3, XPL). Plagioclase harzburgite 899-1: (f) aggregates of Opx2+ (altered) plagioclase developed at the expenses of olivine porphyroclasts (XPL); (g) elongated spinel mantled by altered plagioclase rims (PPL); (h) deep olivine embayments formed at the expenses of porphyroclastic clinopyroxene (XPL).

Fig. 4. Representative microtextural characters of Hole 1070A peridotites: (a) clinopyroxene porphyroclast displaying deep embayment filled by olivine pseudomorphs and tiny extensions propagating into the serpentinized porphyroclastic assemblage (sample 1070-2, PPL); (b) bastitic orthopyroxene rimmed by interstitial secondary olivine (sample 1070-1, XPL); (c) relics of fresh olivine within mesh structures in spinel harzburgite 1070-4 (XPL); (d) brown spinel showing tiny propagation features against olivine-orthopyroxene boundaries (sample 1070-3, PPL).

Fig. 5. Clinopyroxene major element compositions of the investigated samples from the WIM: Cr_2O_3 (wt. %) vs (a) Na_2O (wt. %) and (b) Al_2O_3 (wt. %). Reported fields after Picazo *et al.*, (2016): green = inherited sub-continental mantle; red= refertilized mantle; blue= slow spreading ridge mntle (MAR, Middle Atlantic Ridge).
Light symbols are previous literature data for spinel (black) and plagioclase (red) peridotites from the WIM. Spinel peridotites: cross = Galicia Bank dives (Chazot *et al.*, 2006); triangle = Hole 1068A (Abe, 2001); square = Hole 899B (Chazot *et al.*, 2006); diamond = Hole 897C and 897D (Cornen *et al.*, 1996); circle = Hole 1070A (Abe, 2001; Hébert *et al.*, 2001). Plagioclase peridotites: asterisk = Galicia margin (Kornprobst *et al.*, 1988); triangle = Hole 1068A (Abe, 2001).

Fig. 6. Clinopyroxene major element variations of the analyzed peridotites from the WIM: (a) Al_2O_3 (wt. %) vs Mg#; (b) TiO_2 (wt. %) vs Na_2O (wt. %); (c) Cr_2O_3 vs TiO_2 (wt. %).
Light symbols are previous literature data for the WIM peridotites as reported in Fig. 5.

Fig. 7. Compositional variations of spinel of the investigated WIM peridotites: (a) spinel Cr# vs. Mg#. Field for abyssal and forearc peridotites are from Dick & Bullen (1984) and *Ishii et al.*, (1992), respectively; (b) olivine Mg# vs. spinel Cr#. The olivine-spinel mantle array (OSMA) is shown by dashed lines. Field for supra-subduction zone, abyssal and passive margins peridotites are after Dick & Bullen (1984), Arai (1994), Pearce *et al.*, (2000); (c) spinel Cr# vs. TiO_2 (wt. %). Fields reported with dashed lines as indicated in Fig. 5.
Light black and red symbols are literature data on the WIM peridotites, see Fig. 5 for legend.

Fig. 8. Clinopyroxene trace element patterns of the investigated peridotites from the WIM. Fig. 7 (a)-(c)-(e)-(g): chondrite-normalized REE patterns; Fig. 7 (b)-(d)-(f)-(h): PM-normalized extended trace element patterns. Normalizing values after Sun & McDonough, 1989.
(a) and (b): Hole 1068A plagioclase lherzolites. Blue patterns in (a) = literature data from Abe (2001). Compositional fields reported for comparison are North Lanzo (pink) and Lower Platta (green) from Kaczmarek & Müntener, (2008); Muntener *et al.*, (2010).
(c) and (d): Hole 899B spinel harzburgites. Pale pink field plotted for comparison in (c) represents mantle xenoliths with V-shaped patterns from Eastern Europe (Downes *et al.*, 2003).
(e) and (f): Hole 899 B plagioclase harzburgite. Red pattern (e) = literature data for Hole 899 B plagioclase peridotite (Chazot at al., 2006). Compositional fields are residual abyssal peridotites in grey (Warren, 2016) and impregnated mantle rocks of the Alps-Apennine (IL, Internal

Ligurides: Rampone *et al.*, 1996; S Tuscany, Tribuzio *et al.*, 2004; Corsica, Rampone *et al.*, 2008).

(g) and (h): Hole 1070A spinel peridotites. Grey patterns (g) = Hole 1070 literature data (Abe, 2001). Compositional field reported are peridotites with hump-shaped REE patterns from the SWIR (grey field, Brunelli *et al.*, 2014) and CIR (lilac, Hellebrand *et al.*, 2002; Hellebrand & Snow, 2003).

Fig. 9. Orthopyroxene trace element patterns of the analyzed WIM peridotites. Fig. 9 (a)-(c)-(e): chondrite-normalized REE patterns; Fig. 9 (b)-(d)-(f): PM-normalized extended trace element patterns. Normalizing values after Sun & McDonough, 1989.

(a) and (b): Hole 899B spinel harzburgites. Grey field in (a) is orthopyroxene REE composition of MAR peridotites (Hole 1272A, Secchiari, *unpublished*).

(c) and (d): Hole 899B plagioclase harzburgite. Compositional fields reported for comparison in (c) are impregnated mantle rocks of the Alps-Appenine (see Fig. 7 for references).

(e) and (f): Hole 1070A spinel peridotites.

Fig. 10. Comparison of temperatures derived from the REE-in-two-pyroxene thermometer (T_{REE-Y}, Liang *et al.*, 2013b with temperatures from (a) two-pyroxene thermometer (T_{BKN}, Brey & Köhler, 1990); (b) Ca-in-orthopyroxene thermometer ($T_{Ca-in-Opx,}$ Brey & Köhler, 1990) and (c) olivine-spinel thermometer (T_{Ol-Spl}, Li *et al.*, 1995). Reported for comparison: pink field = abyssal peridotites; grey field = ophiolitic peridotites; pale green field = sub-continental lithospheric mantle (Dygert & Liang, 2015 and references therein; Secchiari *et al.*, 2022).

Fig. 11. Variation of REE ratios (a) Sm_N/Yb_N and (b) Ce_N/Yb_N as a function of Yb_N in clinopyroxene of the WIM peridotites. Grey lines represent the residual compositions calculated for non-modal fractional melting of DMM in the spinel stability field (path 1) and after 7% melting in the garnet stability field followed by melting in the spinel field (path 2). Marks on the melting curves indicate 5% melting increments. Melting curves and SWIR peridotites field after Seyler & Brunelli (2018).

CIRCE93-7= Cpx-poor harzburgite from the CIR (Hellebrand *et al.*, 2002).

Fig. 12. Zr and Sr in clinopyroxene from the WIM peridotites. Curves A and B are batch and fractional melting trends for a spinel peridotite source after Müntener *et al.*, (2010). Red dashed line is the refertilization trend.

Fig. 13. REE refertilization models obtained for plagioclase-bearing samples (a) 1068-2 and (b) 899-1. Starting composition is a depleted spinel peridotite, with HREE compositions similar to spinel harzburgite 899-3, corresponding to 5% fractional melting of a DMM source in the garnet stability field, followed by 4% fractional melting in the spinel field. Dotted lines indicate addition of 2% increments of liquids followed by equilibrium trace element distribution among the phases. The near-fractional model has been obtained by adding 2% increments of: (a) a MORB-type melt; (b) a non-aggregated, depleted melt derived from 4% fractional melting of a DMM-source in the spinel field. Details on the model, including clinopyroxene/melt partition coefficients, are reported in Table 6 in Electronic Supplementary Material.

Fig. 14. Fractional melting model following Norman (1998) based upon Lu_N–Yb_N systematics in clinopyroxene. The model calculates non -modal fractional melting in the spinel stability field starting from a DMM mantle source (Salters & Stracke, 2004). Partition coefficients after Ionov *et al.*, (2002).

Fig. 15. Zr vs Ti (μg/g) in the clinopyroxenes of the WIM compared with non-modal fractional paths after 0 % (spinel field), 5% and 10% partial melting in the garnet field followed by melting in the spinel field. Light grey represents abyssal peridotites field from the work of Brunelli *et al.*, (2006).

Fig. 16. Chondrite-normalized REE patterns of the melts in equilibrium with spinel harzburgites 899-3 and 899-4 calculated using partition coefficients of Hart & Dunn (1993). Normalizing values after Sun & McDonough, 1989.

Fig. 17. Clinopyroxene variation diagrams for Hole 1070A peridotites: (a) Al_2O_3 (wt. %) vs Cr#; (b) Cr# Cpx vs Yb, empty symbols= rims; (c) Na_2O (wt. %) vs. Yb. Pale blue arrow in (c) represents partial melting trend, while grey dashed arrow indicates deviation from the main melting trend and concomitant Na_2O enrichment.

Fig. 18. Melt entrapment model showing clinopyroxene compositions normalized to chondrite (Sun & McDonough, 1989). The model uses a depleted harzburgite starting composition with 5% modal clinopyroxene, which was calculated from 9% fractional melting (5% melting in the garnet field, followed by 4% melting in the spinel stability field) of a DMM source. Compositions of the trapped melt (black line): melt increment derived from 3% fractional melting of a DMM source in the garnet stability field. The grey dotted lines show the evolution

of the resulting clinopyroxene as the melt crystallizes, labeled with the percentage of trapped melt.

Table 1

Sample names and their position in ODP cores

Sample name	Leg	Hole	Core	Section	Interval (cm)	Depht (mbsf)	Rock-type	Primary minerals	Cpx (vol.%)**
899-1	149	899B	20R	4	90-97	412.84	Pl harzburgite	Ol, Opx, Cpx, Sp, Pl	8%
899-2	149	899B	21R	2	62-67	418.86	Serpentinite breccia	Serpentinized*	-
899-3	149	899B	21R	4	80-83	421.76	Spl harzburgite	Ol, Opx, Cpx, Sp	3%
899-4	149	899B	23R	4	55-61	437.56	Spl harzburgite	Ol, Opx, Cpx, Sp	2%
1068-1	173	1068A	27R	3	30-34	943.53	Pl lherzolite	Serpentinized*	-
1068-2	173	1068A	29R	3	70-73	954.21	Pl lherzolite	Cpx, Sp, Pl	10%
1070-1	173	1070A	10R	1	116-119	687.06	Spl harzburgite	Opx, Sp	5%
1070-2	173	1070A	10R	1	134-139	687.24	Spl harzburgite	Opx, Sp	4%
1070-3	173	1070A	12R	1	24-27	705.34	Spl harzburgite	Opx, Cpx, Sp	4%
1070-4	173	1070A	13R	4	104-108	711.61	Spl harzburgite	Ol, Opx, Cpx, Sp	2%

* no primary mantle phases preserved

** estimated

Fig. 1.

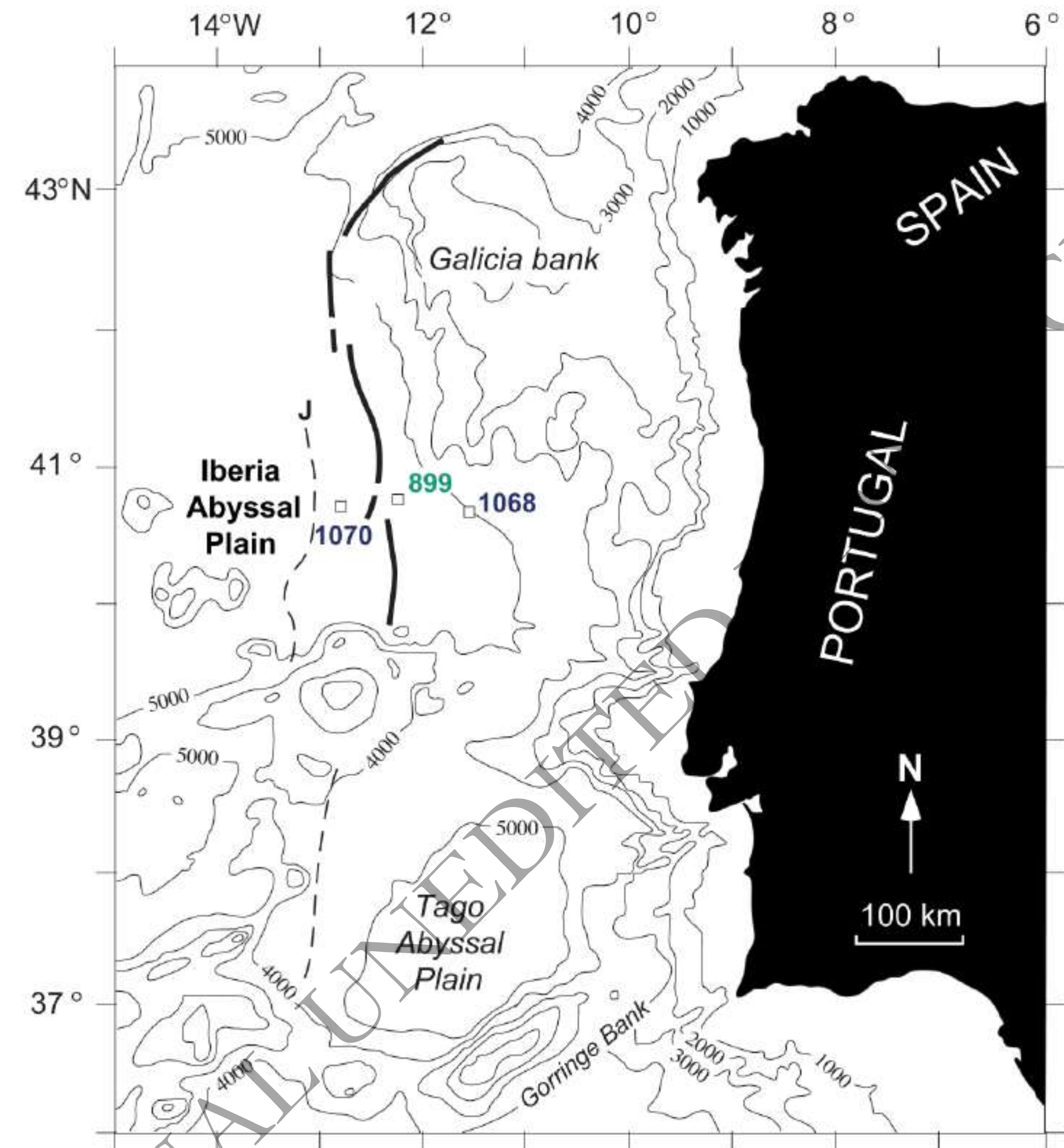
14°W
12°
10°
8°
6°
43°N
41°
39°
37°
5000
4000
3000
2000
1000
Galicia bank
SPAIN
PORTUGAL
J
Iberia
Abyssal
Plain
899
1068
1070
Tago
Abyssal
Plain
Gorringe Bank
N
100 km

Fig. 2.

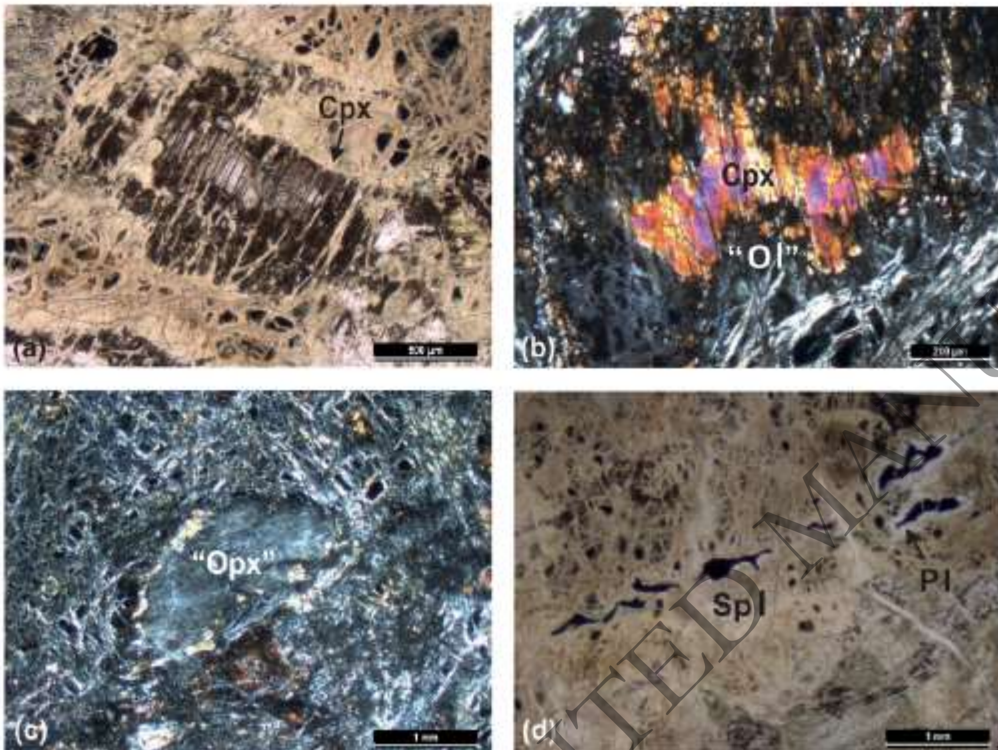

Fig. 3.

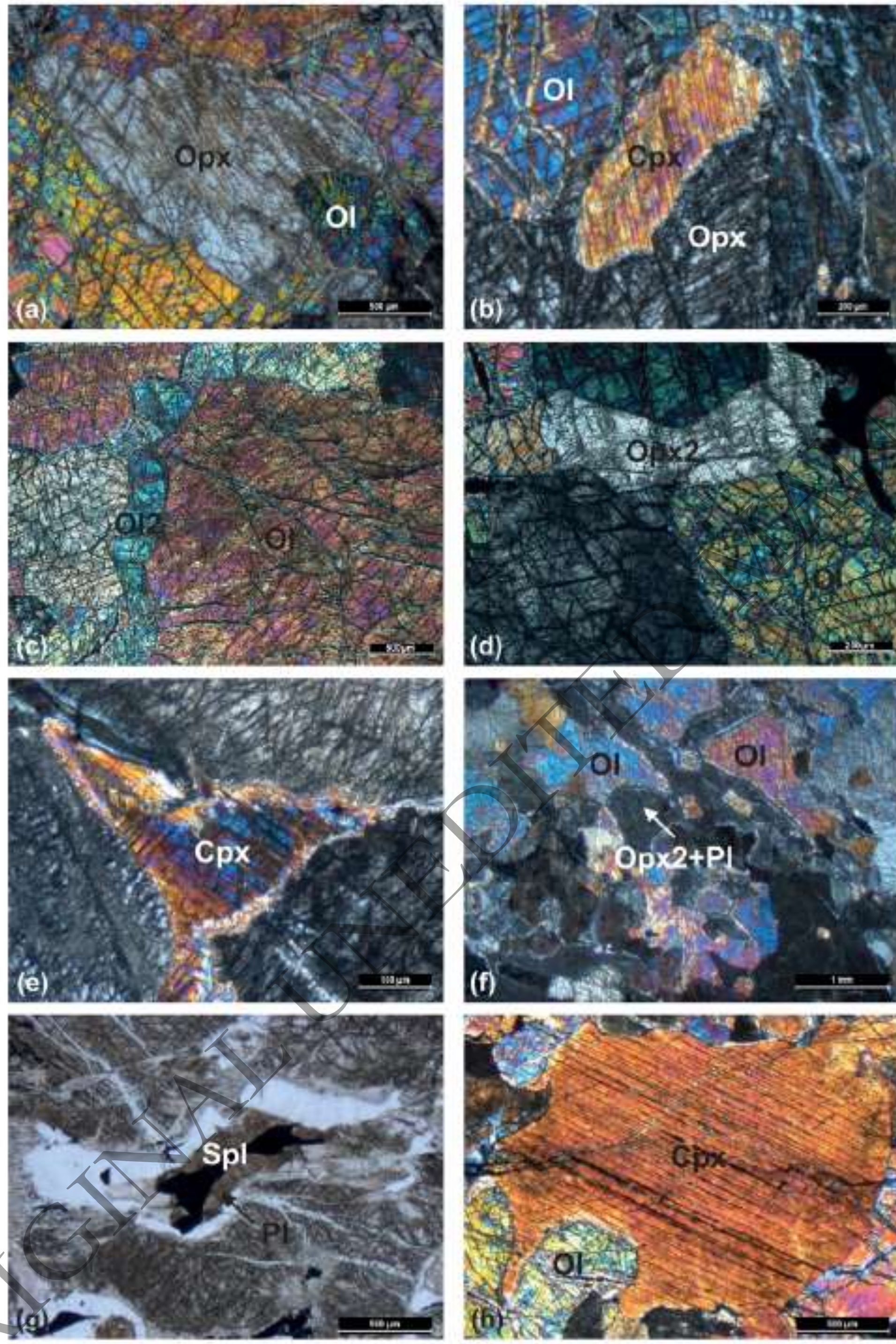
Opx
Ol
(a)
Ol
Cpx
Opx
(b)
Ol2
Ol
(c)
Opx2
Ol
(d)
Cpx
(e)
Ol
Ol
Opx2+Pl
(f)
Spl
Pl
(g)
Cpx
Ol
(h)

Fig. 4.

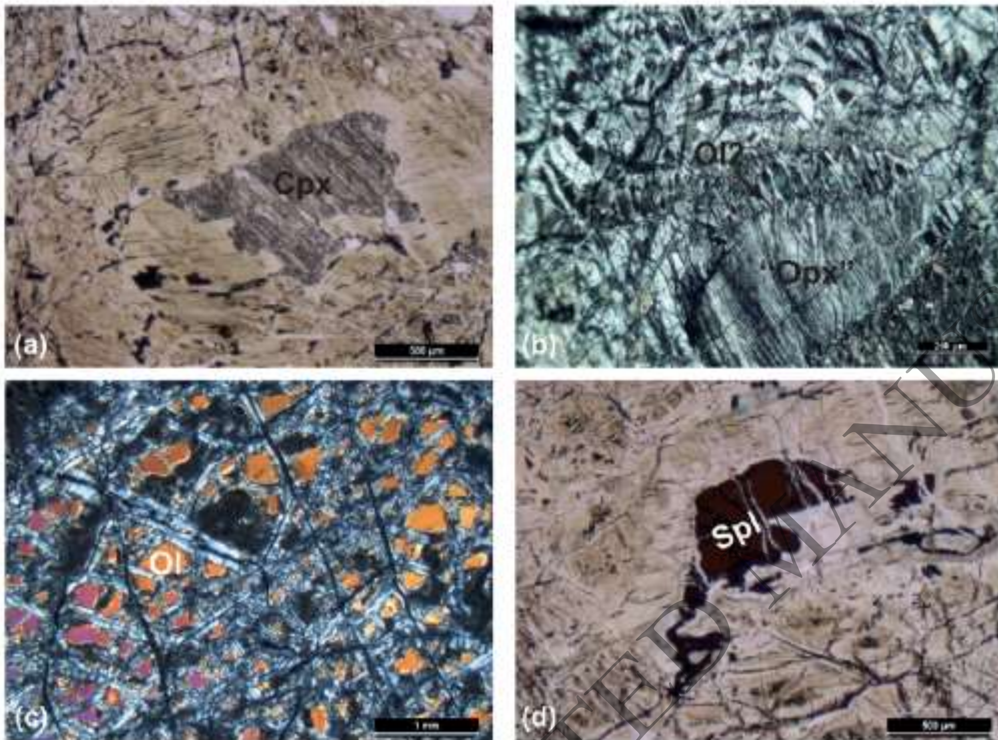
Cpx
(a)
Ol?
"Opx"
(b)
Ol
(c)
1 mm
Spl
(d)

Fig. 5.

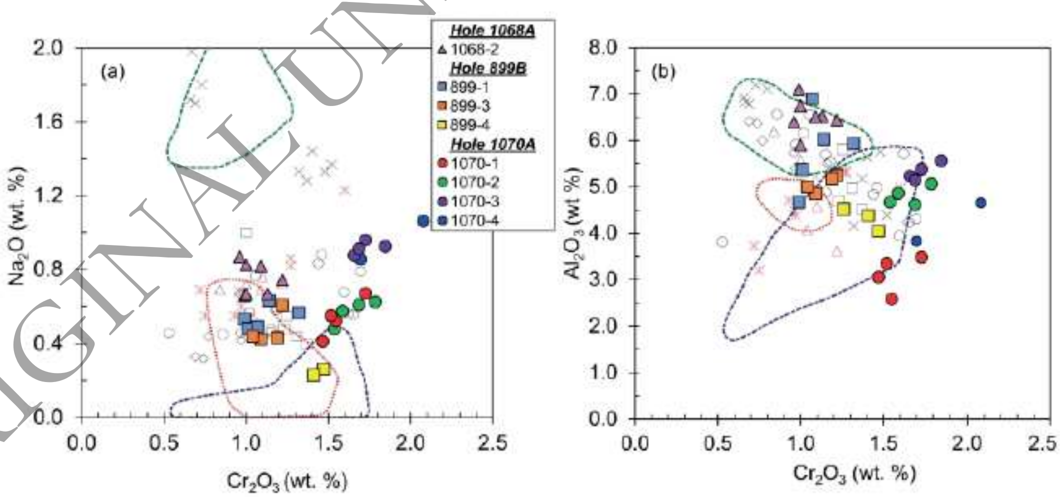
(a)
(b)
Na2O (wt. %)
Al2O3 (wt %)
Cr2O3 (wt. %)
Hole 1068A
1068-2
Hole 899B
899-1
899-3
899-4
Hole 1070A
1070-1
1070-2
1070-3
1070-4

Fig .6.

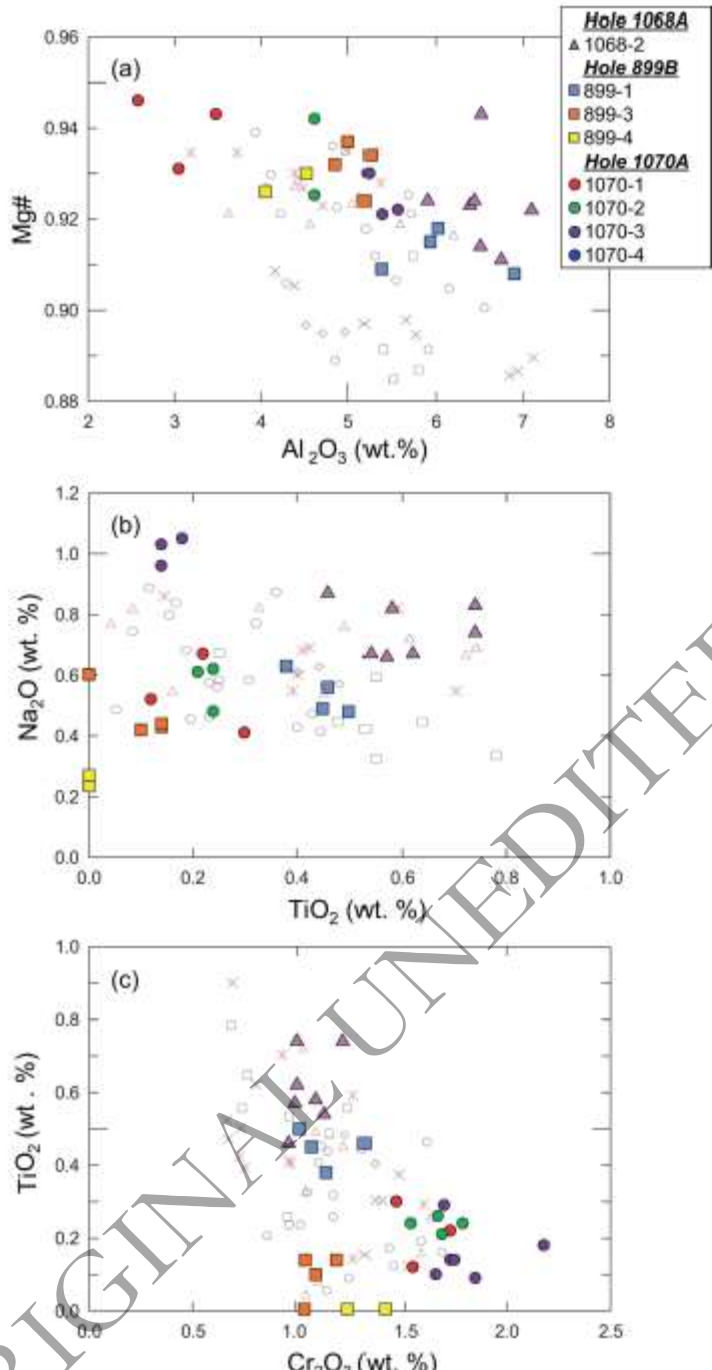
Hole 1068A
1068-2
Hole 899B
899-1
899-3
899-4
Hole 1070A
1070-1
1070-2
1070-3
1070-4
(a)
Mg#
Al_2O_3 (wt.%)
(b)
Na_2O (wt. %)
TiO_2 (wt. %)
(c)
TiO_2 (wt . %)
Cr_2O_3 (wt. %)

Fig. 7.

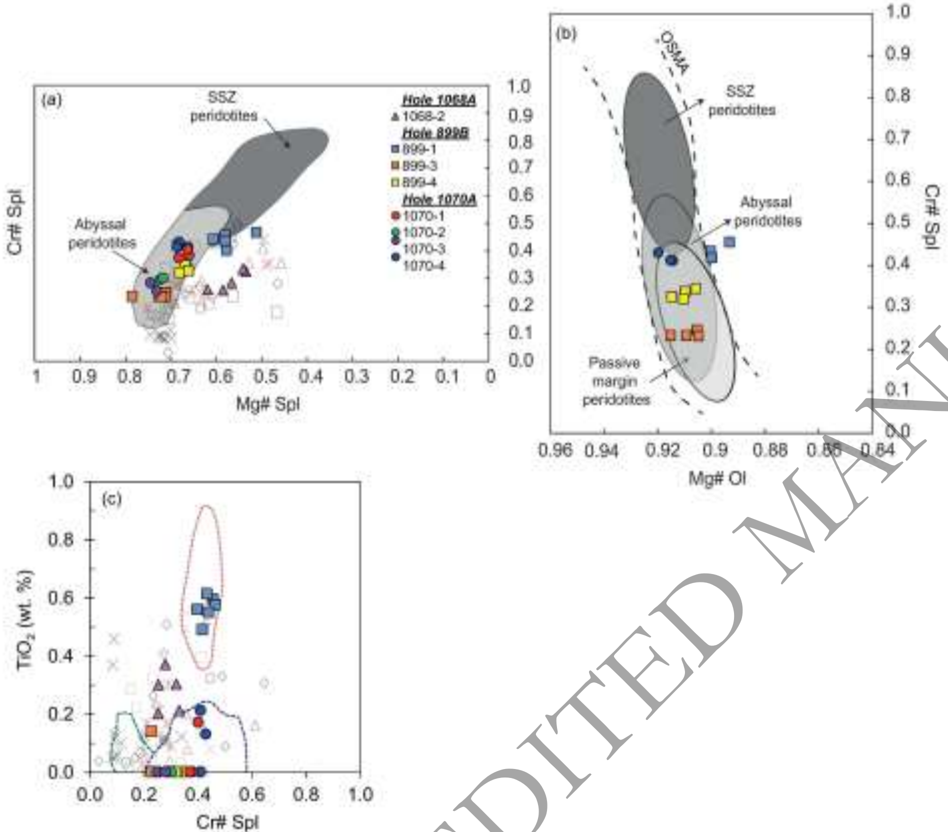
(a)
SSZ peridotites
Abyssal peridotites
Hole 1068A
1068-2
Hole 899B
899-1
899-3
899-4
Hole 1070A
1070-1
1070-2
1070-3
1070-4
Cr# Spl
Mg# Spl
(b)
OSMA
SSZ peridotites
Abyssal peridotites
Passive margin peridotites
Cr# Spl
Mg# Ol
(c)
TiO2 (wt. %)
Cr# Spl

Fig. 8.

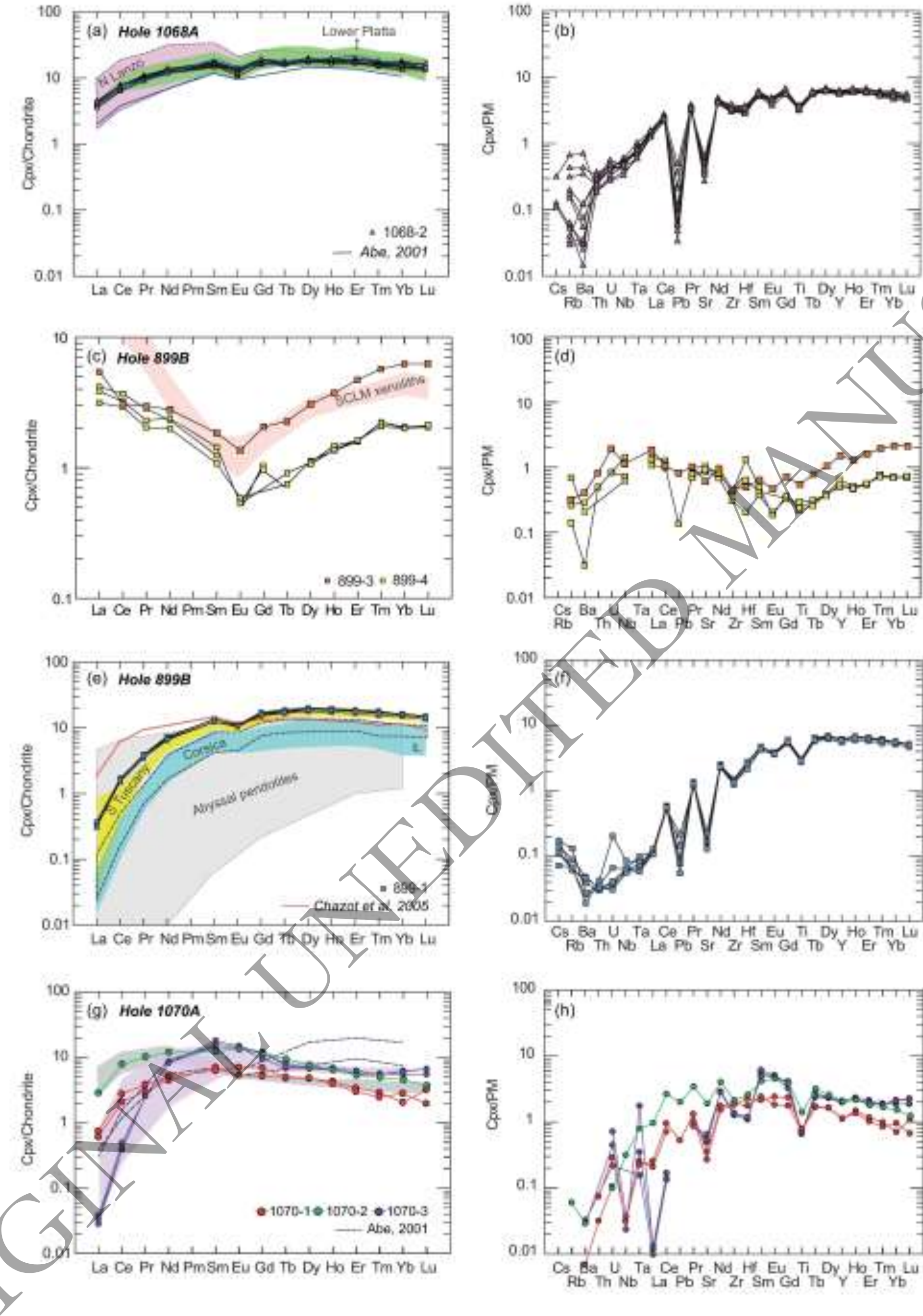

(a) Hole 1068A
N Lanzo
Lower Platta
1068-2
Abe, 2001
Cpx/Chondrite
La Ce Pr Nd Pm Sm Eu Gd Tb Dy Ho Er Tm Yb Lu
(b)
Cpx/PM
Cs Rb Ba Th U Nb Ta La Ce Pb Pr Sr Nd Zr Hf Sm Eu Gd Ti Tb Dy Y Ho Er Tm Yb Lu
(c) Hole 899B
SCLM xenoliths
899-3 899-4
(d)
(e) Hole 899B
S Tuscany
Corsica
Abyssal peridotites
899-1
Chazot et al. 2005
(f)
(g) Hole 1070A
1070-1 1070-2 1070-3
Abe, 2001
(h)

Fig. 9.

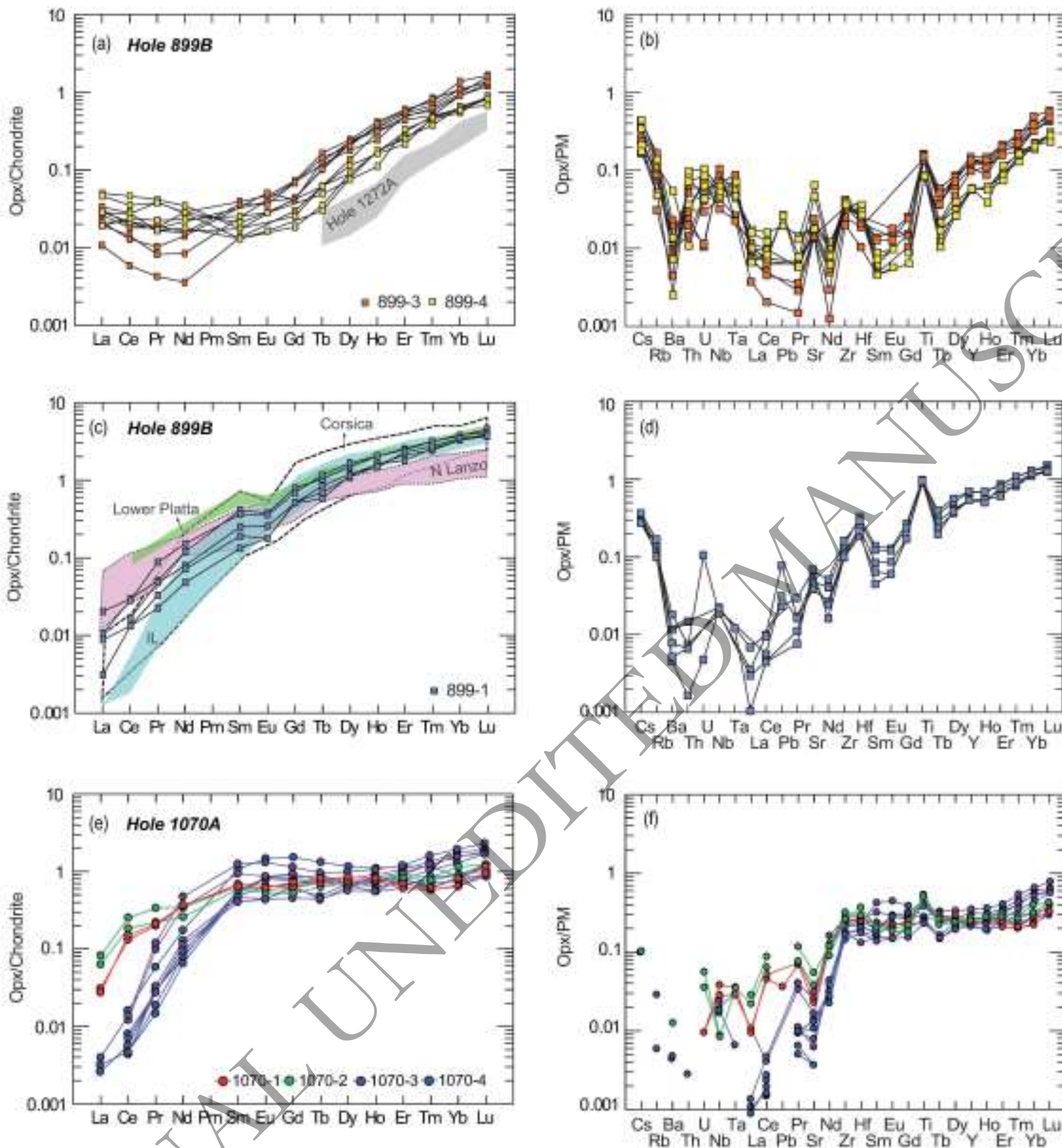

(a) Hole 899B
Opx/Chondrite
Hole 1272A
899-3
899-4
La Ce Pr Nd Pm Sm Eu Gd Tb Dy Ho Er Tm Yb Lu
(b)
Opx/PM
Cs Rb Ba Th U Nb Ta La Ce Pb Pr Sr Nd Zr Hf Sm Eu Gd Ti Tb Dy Y Ho Er Tm Yb Lu
(c) Hole 899B
Corsica
N Lanzo
Lower Platta
IL
899-1
(d)
(e) Hole 1070A
1070-1
1070-2
1070-3
1070-4
(f)

Fig. 10.

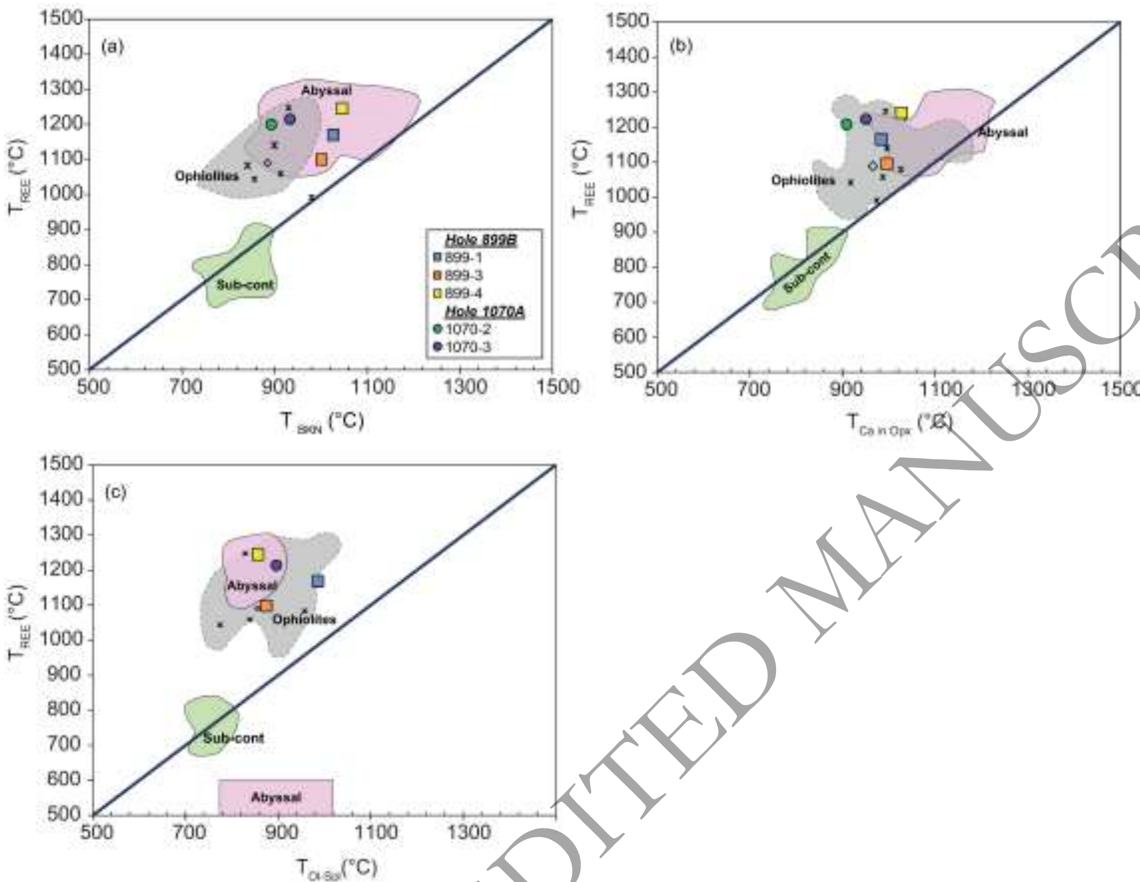
(a)
Abyssal
Ophiolites
Sub-cont
Hole 899B
899-1
899-3
899-4
Hole 1070A
1070-2
1070-3
T REE (°C)
T BKN (°C)
(b)
Abyssal
Ophiolites
Sub-cont
T REE (°C)
T Ca in Opx (°C)
(c)
Abyssal
Ophiolites
Sub-cont
Abyssal
T REE (°C)
T Ol-Spl (°C)

Fig. 11.

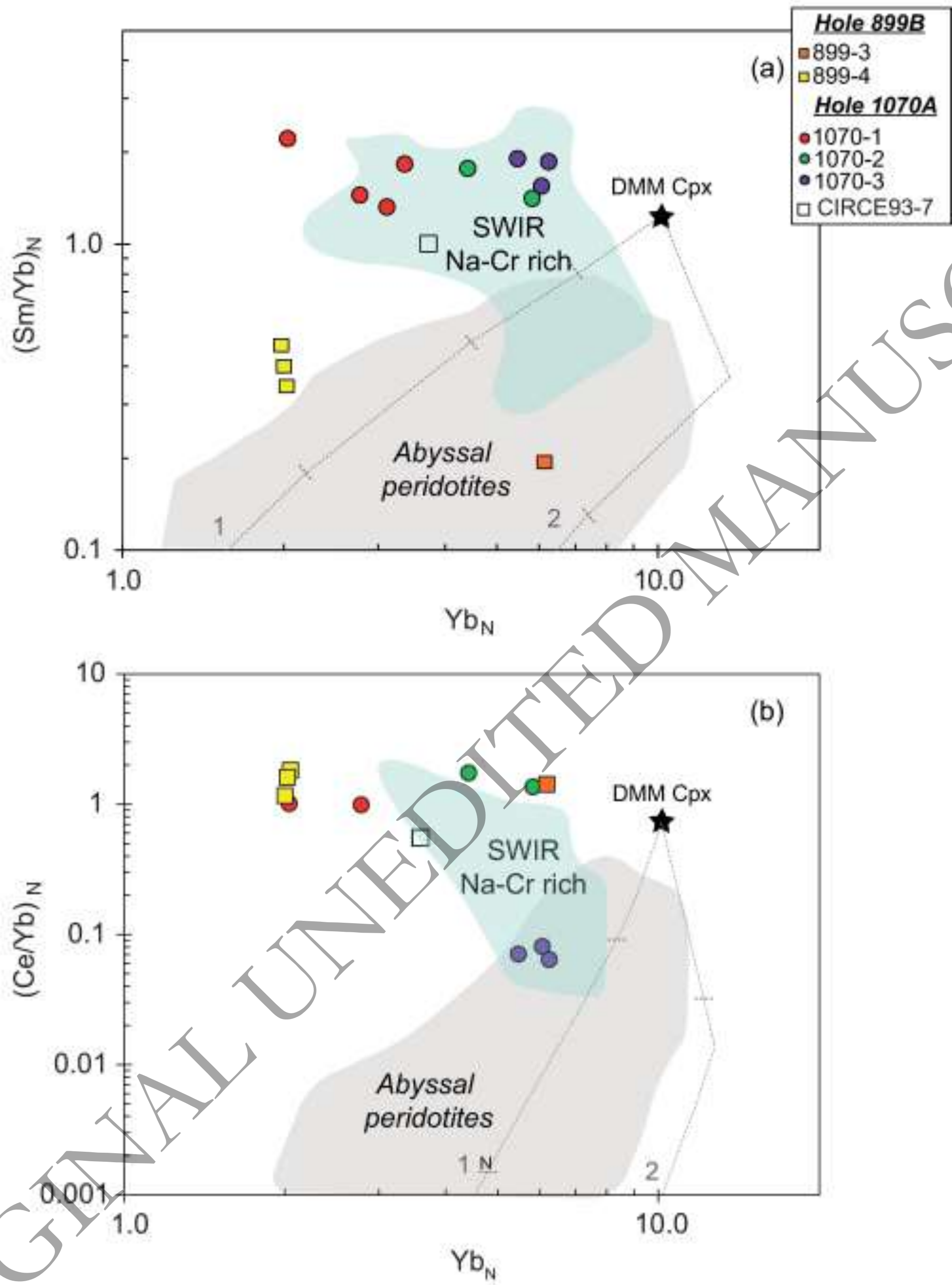
Hole 899B
899-3
899-4
Hole 1070A
1070-1
1070-2
1070-3
CIRCE93-7
(a)
DMM Cpx
SWIR
Na-Cr rich
Abyssal
peridotites
1
2
(Sm/Yb)N
YbN
1.0
0.1
1.0
10.0
(b)
DMM Cpx
SWIR
Na-Cr rich
Abyssal
peridotites
(Ce/Yb)N
YbN
10
1
0.1
0.01
0.001
1.0
10.0

Fig. 12.

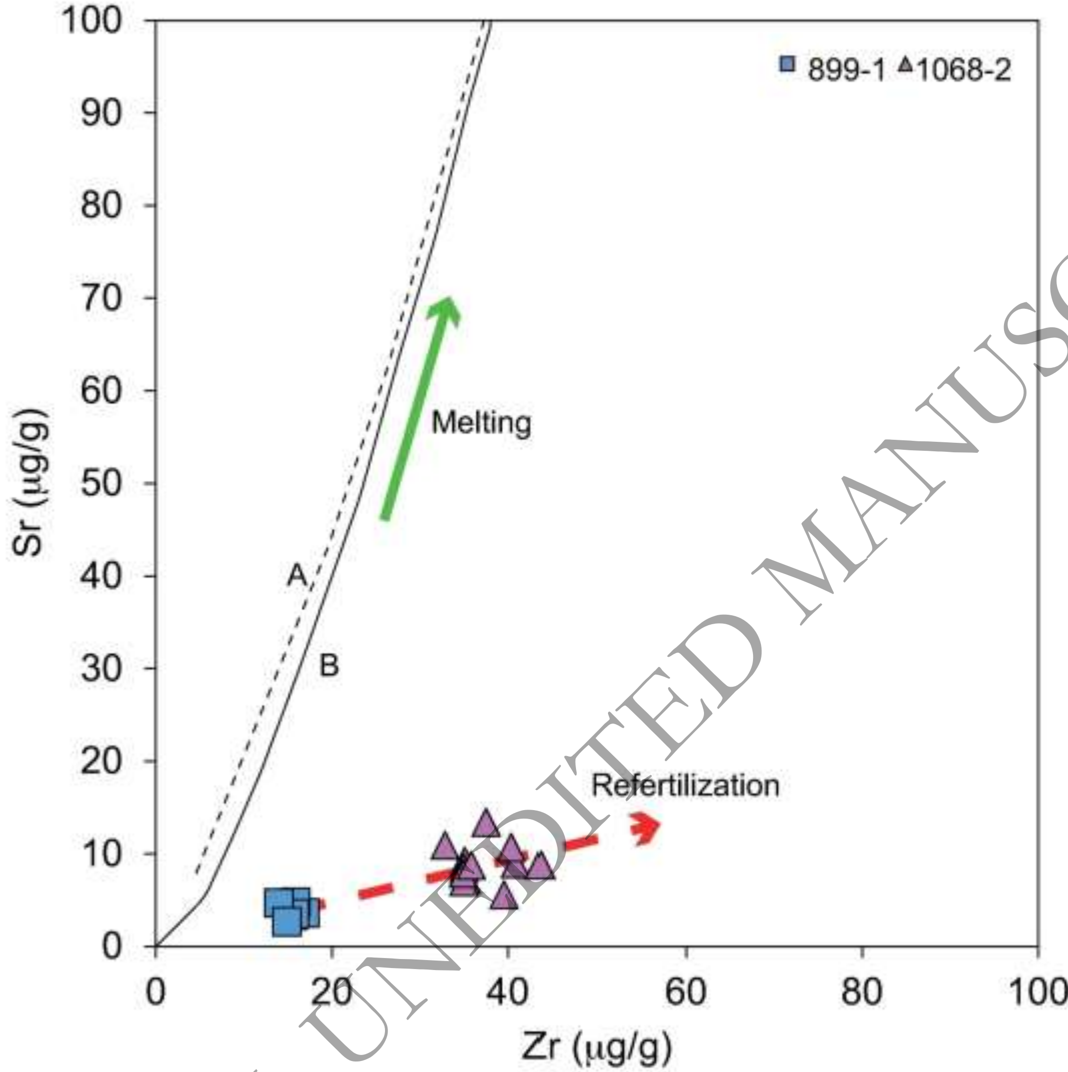
899-1 1068-2
Melting
Refertilization
A
B
Sr (µg/g)
Zr (µg/g)
0
10
20
30
40
50
60
70
80
90
100
0
20
40
60
80
100

Fig. 13.

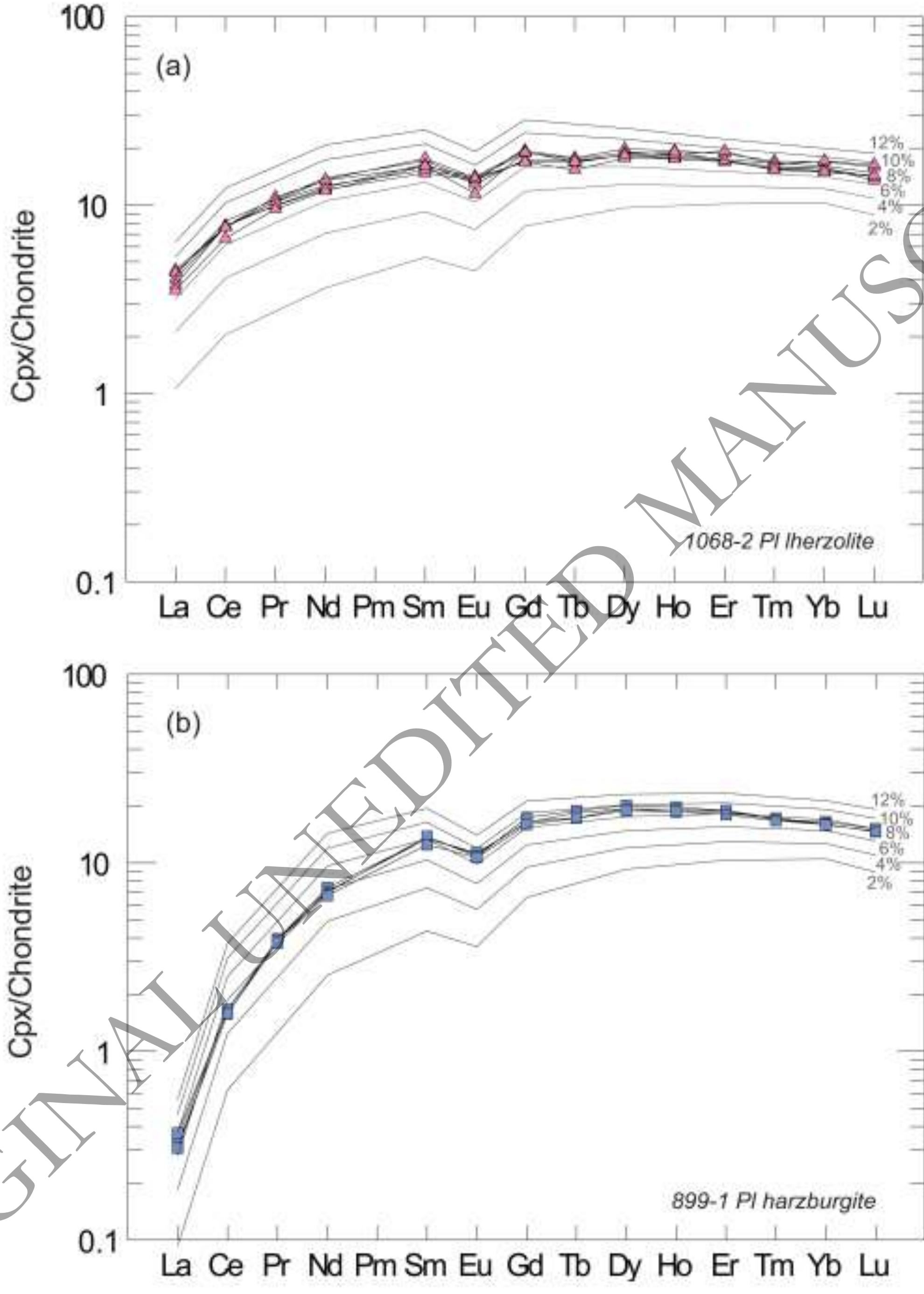
100
10
1
0.1
Cpx/Chondrite
(a)
12%
10%
8%
6%
4%
2%
1068-2 Pl lherzolite
La Ce Pr Nd Pm Sm Eu Gd Tb Dy Ho Er Tm Yb Lu
(b)
899-1 Pl harzburgite

Fig. 14.

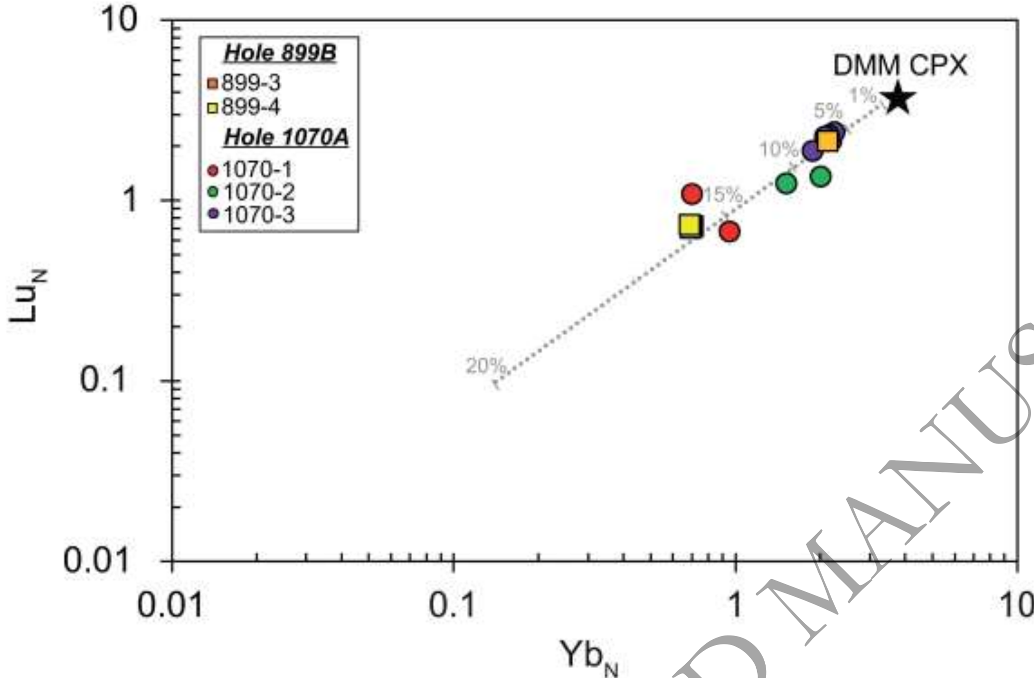
Hole 899B
899-3
899-4
Hole 1070A
1070-1
1070-2
1070-3
DMM CPX
1%
5%
10%
15%
20%
Lu_N
Yb_N
10
1
0.1
0.01
0.01
0.1
1
10

Fig. 15.

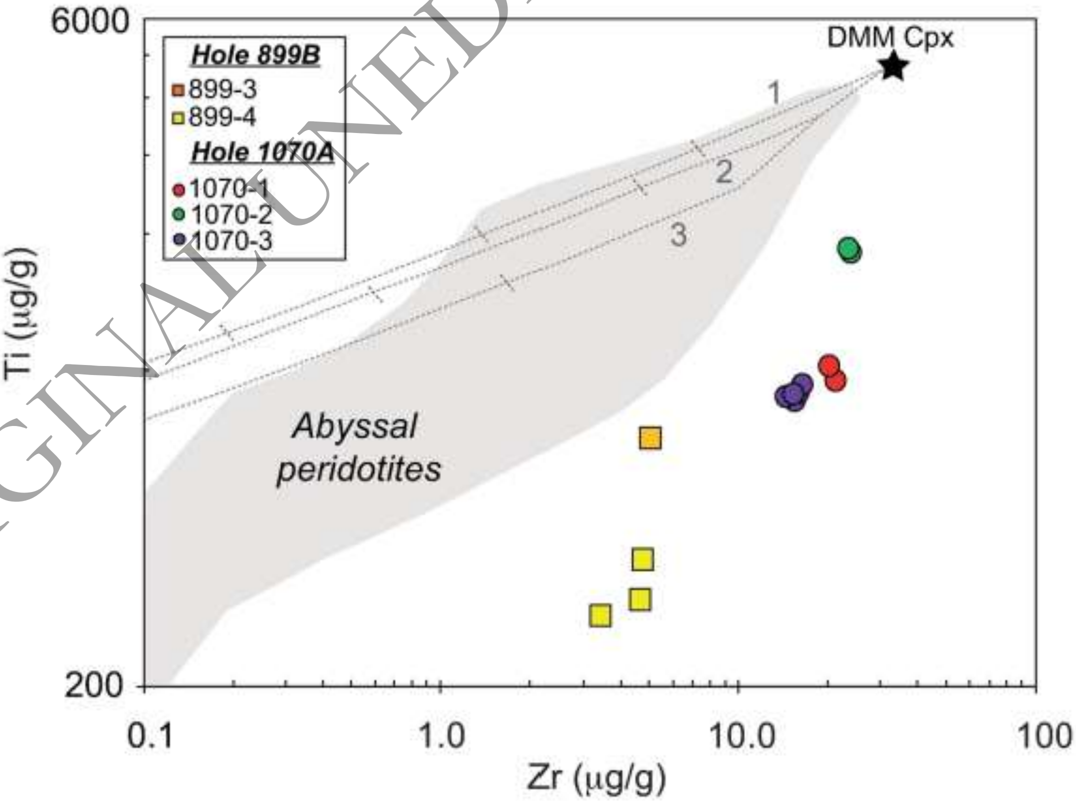
Hole 899B
899-3
899-4
Hole 1070A
1070-1
1070-2
1070-3
DMM Cpx
1
2
3
Abyssal peridotites
Ti (μg/g)
Zr (μg/g)
6000
200
0.1
1.0
10.0
100

Fig. 16.

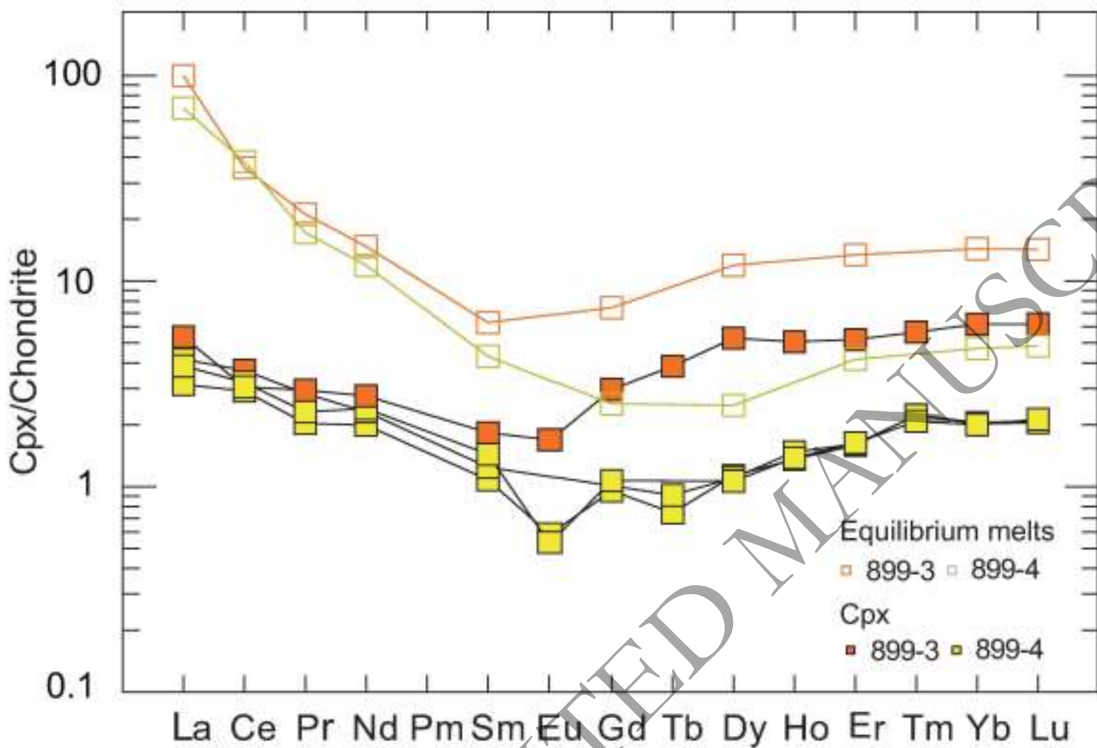
Cpx/Chondrite
100
10
1
0.1
La Ce Pr Nd Pm Sm Eu Gd Tb Dy Ho Er Tm Yb Lu
Equilibrium melts
899-3 899-4
Cpx
899-3 899-4

Fig. 17.

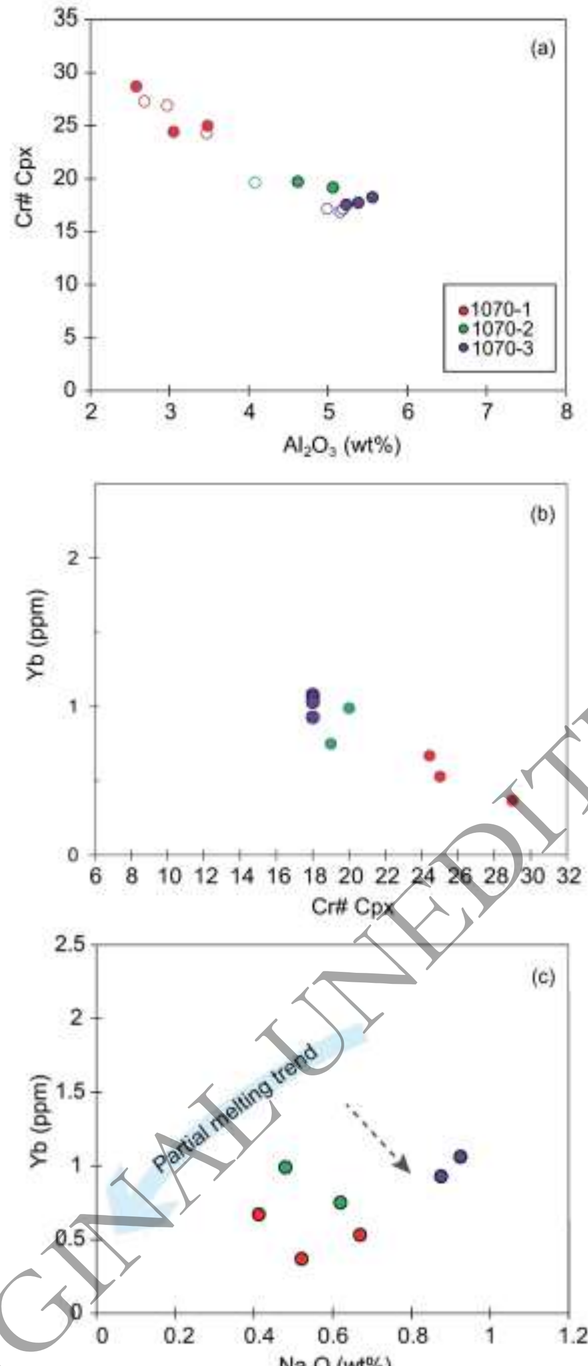

(a)
Cr# Cpx
Al2O3 (wt%)
1070-1
1070-2
1070-3
(b)
Yb (ppm)
Cr# Cpx
(c)
Partial melting trend
Yb (ppm)
Na2O (wt%)

Fig. 18.

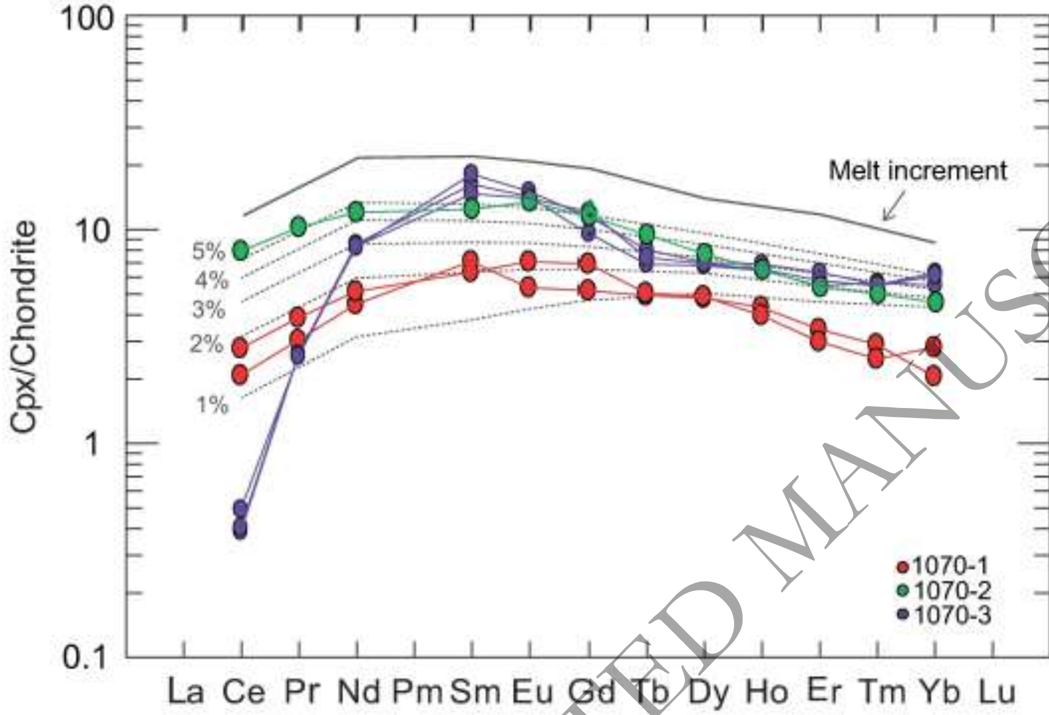
100
10
1
0.1
Cpx/Chondrite
Melt increment
5%
4%
3%
2%
1%
1070-1
1070-2
1070-3
La
Ce
Pr
Nd
Pm
Sm
Eu
Gd
Tb
Dy
Ho
Er
Tm
Yb
Lu